Fast Self-Stable Planar Bipedal Running

by

Maarten J. van den Broek

to obtain the degree of Master of Science
at the Delft University of Technology,
to be defended publicly on August 27, 2019 at 14:00.

Student number:	4140575	
Project duration:	October 1, 2018 – June 24, 2019	
Thesis committee:	Prof. Dr.-Ing. H. Vallery	TU Delft, supervisor
	Prof. Dr. Ir. M. Wisse	TU Delft
	Bram Sterke	TU Delft
	Dr. J. Pratt	IHMC, supervisor
	Dr. R. Griffin	IHMC, supervisor

An electronic version of this thesis is available at `http://repository.tudelft.nl/`.

TU Delft ihmc ROBOTICS

Preface

This thesis is the culmination of my studies in Delft and abroad. It builds on the things I have learnt and the experiences I have come to gather. Many thanks to all those that I can call friends for their support and to those that have taught me for imparting their knowledge.

I would like to specifically thank Jerry Pratt, Robert Griffin, Sylvain Bertrand, and the rest of the robotics lab for their support in performing this research that has come to be my thesis - you were good colleagues and good friends. Furthermore, thanks to Heike Vallery for her critical feedback and supervision from the TU Delft.

Finally, I am grateful to my parents for supporting me troughout my studies and to Vera for always being by my side, even if an ocean separated us at times.

I hope this will prove an interesting read and am proud to share my work.

Maarten J. van den Broek
Delft, August 2019

Contents

I

Fast Self-Stable Planar Bipedal Running

Maarten J. van den Broek, Chris Schmidt-Wetekam, Johnny Godowski,
Ken Chao, Robert Griffin, Jerry Pratt

Paper to be published.

Abstract

Bipedal running gaits may be self-stable if they rely on the intrinsic system dynamics to attenuate deviations. This use of passive dynamics for gait stability has been observed in biological running and applied for running robotics, supported with the results of numerical simulations. It is an important aspect of the development of fast and agile legged robotic locomotion over complex terrain. One part of running stability, trunk stabilization, can be described using a virtual pendulum model. We believe such a metacentric model may be applied in robotic design to achieve passive stabilization of body pitch for fast bipedal running.

In this study, we test metacentric models for self-stabilization of body pitch in bipedal running and evaluate the effects of running speed, design parameter variations, and control strategies. We extract data from experiments with the Planar Elliptical Runner and compare these with a planar spring-loaded inverted pendulum model with a trunk (TSLIP).

We find passive self-stable gaits in the TSLIP model with the centre of mass below the hip. These gaits demonstrate robustness to disturbances and do not require inertial measurements or high-gain feedback control. At high velocities, foot placement and choice of leg stiffness become less critical for gait stability. Data from experiments with the Planar Elliptical Runner support the findings from the model behaviour as it runs reliably, with passively stable body pitch, and without feedback control.

A metacentric model, such as the virtual pendulum model, may explain the observed passive body-pitch stabilization. Evidence from the model ground reaction forces suggests that pitch stability for the Planar Elliptical Runner can also be explained with a metacentric model. Stability in height and velocity can be explained with the compliant leg behaviour in stance.

Constructing a metacentre through mechanical design is beneficial to intrinsic body-pitch stability and subsequently facilitates full gait self-stability in fast running robotics. Implicit feedback allows off-loading of high-gain feedback control onto the system mechanical design, thus contributing to developments for fast legged locomotion over rough terrain.

1 Introduction

Legged locomotion has a high potential for fast and agile movement over uneven terrain. However, fast and efficient running robots have been elusive, in part because of hardware limitations. We believe that tuned intrinsic dynamics can facilitate fast running through mechanical design and therefore seek to explore what makes bipedal running stable and robust.

1.1. Background

Intermittent contact and the ability to deal with complex terrain allows humans, animals, and robots with legs to go where wheeled access is hard (Palmer et al., 2014). Moving fast on legs requires running, which is a natural progression from a walking gait as the required speed increases, marked by the gait featuring a stance and a flight phase (McGeer, 1990).

During running, we can discern between high-level control for path planning and conscious obstable negotiation and low-level control for gait generation and unplanned perturbation handling. In this work, we characterize the low-level gait behaviour with measures of robustness and stability, where robustness is defined as the ability of the running system to not fall in response to large disturbances and stability is defined as the limit-cycle behaviour to small perturbations in the system state.

Running gaits are global limit cycles which are a function of control patterns, system dynamics, and the environment (Taga et al., 1991). These are considered self-stabilizing if they rely on intrinsic system dynamics for attenuating deviations from the periodic orbit without directly measuring these errors. Open-loop control signals may be applied, but self-stability is primarily an emergent effect from mechanical parameters (Hackert et al., 2006). Passive system dynamics with hip and leg compliance form a morphological controller through interaction with the environment. This passive generation of low-level gait dynamics provides a basis for simplification of high-level actuated control (Owaki et al., 2011). Mechanical intelligence embedded in the robot morphology leaves computational effort for global planning and special manoeuvres (Mombaur, 2009; Cotton et al., 2012), however, relying on passive dynamics for running efficiency may limit the speed and power with which a robot can respond to disturbances if that is not considered in the mechanical design (Ahmadi and Buehler, 2006).

An example of self-stable gait generation is found in the passive-dynamic runners developed by McGeer (1990) and Owaki et al. (2011), that are powered only by gravity along a down-

ward slope. The interaction of their mechanical design and dynamics with the environment creates an implicit feedback loop, requiring no explicit control. However, their efficiency is offset by the limited set of initial conditions that result in stable running, leading to a lack of robustness to disturbances. Robots such as the single-legged hoppers described by Raibert (1986) or Ahmadi and Buehler (2006) show highly dynamical gaits based on passive dynamics using pneumatic actuation.

The use of passive dynamics for running gaits is also present in biological running. Running birds may use intrinsic dynamics for stability to manage neuromuscular delays at state transitions (Blum et al., 2014) and humans and birds can adapt leg stiffness for negotiation of unobserved rough terrain (Andrada et al., 2013; Birn-Jeffery et al., 2014).

The use of self-stable, passive gait generation has inspired a number of fast running robots. The IHMC FastRunner project achieves high speeds in simulation by applying self-stability and implicit feedback through mechanical design to attain fast, efficient, and robust running (Cotton et al., 2012). The KAIST Raptor demonstrates fast planar bipedal running up to $12.8\,\mathrm{m\,s^{-1}}$ on a treadmill with a tail for pitch stabilization. It has a leg design similar to Kim et al. (2014), using linkages and elastic elements to drive the gait pattern. The IHMC Planar Elliptical Runner robot experimentally realizes fast running in the sagittal plane without explicit sensing, controlled only by motor voltage set by a human operator.

Numerical methods may be used to find the control inputs and mechanical parameters required for open-loop controlled, self-stabilizing bipedal running in both a simple bipedal model with telescoping legs (Mombaur et al., 2005) and for a planar humanoid model (Mombaur, 2009). These do not necessarily improve understanding of the design for passive gait generation.

A simpler model may provide more insight into design for self-stable gaits. One often-used model is the standard spring-mass model (Blickhan, 1989) which represents a spring-loaded inverted pendulum (SLIP). It has been shown to have self-stable limit cycles, requiring no feedback control if started from suitable initial conditions (Seyfarth et al., 2002; Ghigliazza et al., 2003). It is frequently used to model the dynamics of the centre of mass for biological running (Geyer et al., 2006) and it provides a basis for simulation studies investigating the fundamental effects of model parameters such as non-linear leg stiffness (Karssen and Wisse, 2011) or swing-leg retraction in flight (Blum et al., 2011, 2014; Karssen et al., 2015).

Additionally, the SLIP model can be applied for robotic control and design. The self-stable behaviour of the SLIP model is largely conserved as it is extended to a two-legged model (Peuker et al., 2012). It has also facilitated experimental bipedal running robots. For example, ATRIAS was mechanically designed to represent spring-mass model dynamics (Hubicki et al., 2016), whereas robots such as RABBIT (Morris et al., 2006) and MABEL (Grizzle et al., 2009) have their dynamics anchored to spring-mass models through Hybrid Zero Dynamics control (Poulakakis and Grizzle, 2009).

SLIP self-stability covers height and velocity stabilization but for stable running according to the three-part control for running robotics (Raibert, 1986), body pitch needs to be additionally stabilized.

Metacentric stability models may explain passive pitch stabilization. The virtual pendulum model of pitch stability suggests the ground reaction forces may form a metacentre from which the centre of mass is suspended. The body pitch would then naturally stabilize as would a hanging pendulum (Maus et al., 2008, 2010), illustrated in Figure 1.1 (a). For this model to

be valid, the ground reaction forces in body coordinates should remain mostly unchanged in response to pitch disturbance, so that the metacentre is maintained. Otherwise, the ground reaction reaction forces may either not correct the disturbance, or move to generate an over-correcting torque.

A metacentric buoyancy model compares pitch stability in running to a ship in water as illustrated in Figure 1.1 (c). The centre of buoyancy of the vessel shifts more than the centre of mass as the vessel rolls. This results in a restoring torque that stabilizes the vessel in its upright position. Its behaviour is similar to that of the virtual pendulum model. Similarly, as described by Ringrose (1997) explaining self-stability, a wheel with an off-centre mass, shown in Figure 1.1 (b), will stabilize with the centre of mass in the downward position because the ground reaction forces provide a restoring torque.

The SLIP model may be expanded with a trunk to capture the problem of body-pitch stabilization. Such a model is used by Sharbafi et al. (2013) to demonstrate that a passive hip-spring configuration can stabilize pitch similar to a virtual-pivot-point (VPP) controller. A similar model was used by van Oijen et al. (2013) to show that having a centre of mass on the hip is not optimal for the maximum one- or two-step controllable disturbance despite the success of the traditional SLIP model. This suggests the addition of a trunk may be beneficial for running robustness.

This paper aims to explain what makes the Planar Elliptical Runner self-stable and robust. To that end, it features a simulation study with a planar spring-loaded inverted pendulum model with a trunk (TSLIP) and experimental measurements of the running robot. The use of metacentric stability principles for trunk self-stabilization is investigated, as well as mechanical properties for stable and robust fast bipedal running.

1.2. Research Questions

The similarity between the Planar Elliptical Runner robot and the TSLIP model leads us to expect that the model results may provide explanations for the open-loop stable running behaviour on the robot.

We hypothesize that having the centre of mass offset below a physical hip point makes running inherently more stable and robust. This is expected to stabilize pitch by forming a metacentre similar to a VPP controller, illustrated in Figure 1.1. Running with control without explicit inertial reference should then be possible. On the basis of stable pitch, height and velocity can be additionally stabilized without damping. We expect the choice of touch-down angle and leg stiffness to become less critical at higher running speeds. Adding damping to the leg or the hip will likely improve stability and robustness.

1.3. Structure

Section 2 introduces the TSLIP model for bipedal running. This model is used for the simulation study as described in Section 3, for which results are summarized in Section 4.

The design of the Planar Elliptical Runner and the experimental methods are provided in Section 5, with the results presented in Section 6.

The results of the simulation study and the experimental study are discussed in Section 7, followed by the conclusions in Section 8.

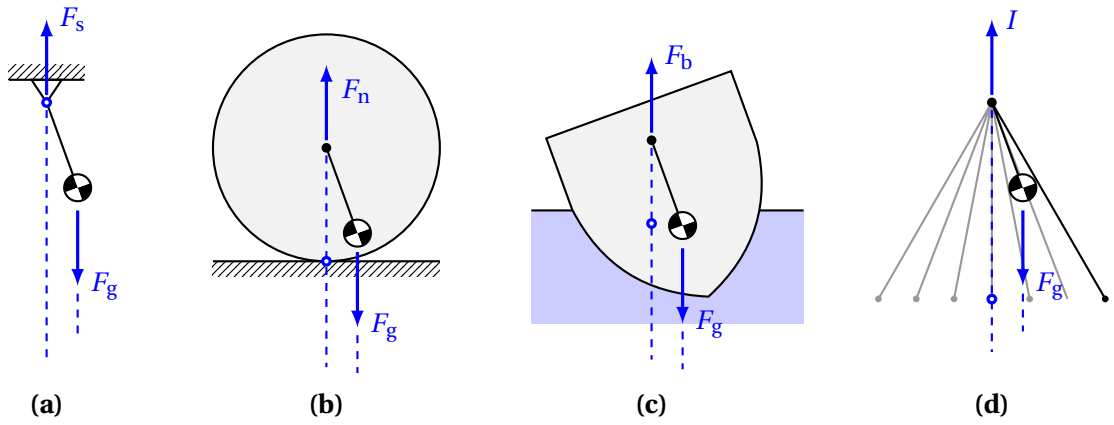

Figure 1.1: Illustration of the metacentric model for pitch stability. All four configurations generate a restoring torque about the centre of mass when a disturbance in pitch angle is applied. **(a)** shows the pitch response for a simple hanging pendulum, with a supporting force F_s and gravitational force F_g. **(b)** illustrates how a wheel with an offset centre of mass has similar behaviour through the normal ground reaction force F_n. **(c)** shows how a floating ship forms a virtual metacentre through the movement of with the buoyancy force F_b, which is applied at the centre of buoyancy. **(d)** shows the approximate pitch response of the TSLIP model, with the resultant ground reaction impulse $\boldsymbol{I}$. This ground impulse remains directed approximately towards the hip, thereby providing the required restoring torque for pitch stability. A detailed model response is provided in Figure 4.2 for the TSLIP model with local velocity control and in Figure 6.2 for the TSLIP model tuned to the measurements of the Planar Elliptical Runner.

2

Description of the Running Model

2.1. Model Definition

The planar spring-loaded inverted pendulum with a trunk (TSLIP) is used to model running in the sagittal plane. It has a massless leg and foot and a linear spring-damper in the leg. The addition of a trunk allows analysis of pitch dynamics. The model definition is illustrated in Figure 2.1 (a).

The forces in the model are illustrated in the free-body diagram in Figure 2.1 (b). The hip torque τ is determined by a control strategy as described in Section 2.4. The compressive leg force F_l is determined with a linear stiffness k and a linear damping coefficient c_l,

$$F_\mathrm{l} = k(l_0 - l) - c_\mathrm{l}\dot{l}, \tag{2.1}$$

where l_0 is the resting leg length, l is the leg length, and $\dot{l}$ is the leg velocity.

2.2. Equations of Motion

In stance phase, the foot is fixed and the entire system can be described with the minimal coordinate vector $\boldsymbol{q}$,

$$\boldsymbol{q} = \begin{bmatrix} l & \beta & \phi \end{bmatrix}^\mathrm{T}. \tag{2.2}$$

The equations of motion can be solved for the generalized accelerations $\ddot{\boldsymbol{q}}$ in stance,

$$\mathbf{M}\ddot{\boldsymbol{q}} = \boldsymbol{Q} - \boldsymbol{C}, \tag{2.3}$$

where $\mathbf{M}$ is the mass matrix in minimal coordinates,

$$\mathbf{M} = \begin{bmatrix} m & 0 & -mr\cos(\beta+\phi) \\ 0 & ml^2 & mrl\sin(\beta+\phi) \\ -mr\cos(\beta+\phi) & mrl\sin(\beta+\phi) & J+mr^2 \end{bmatrix}, \tag{2.4}$$

the vector $\boldsymbol{Q}$ contains the forces in minimal coordinates,

$$\boldsymbol{Q} = \begin{bmatrix} -mg\sin(\beta) + k(l_0 - l) - c_\mathrm{l}\dot{l} \\ \tau - mgl\cos(\beta) \\ \tau - mgr\sin(\phi) \end{bmatrix},$$

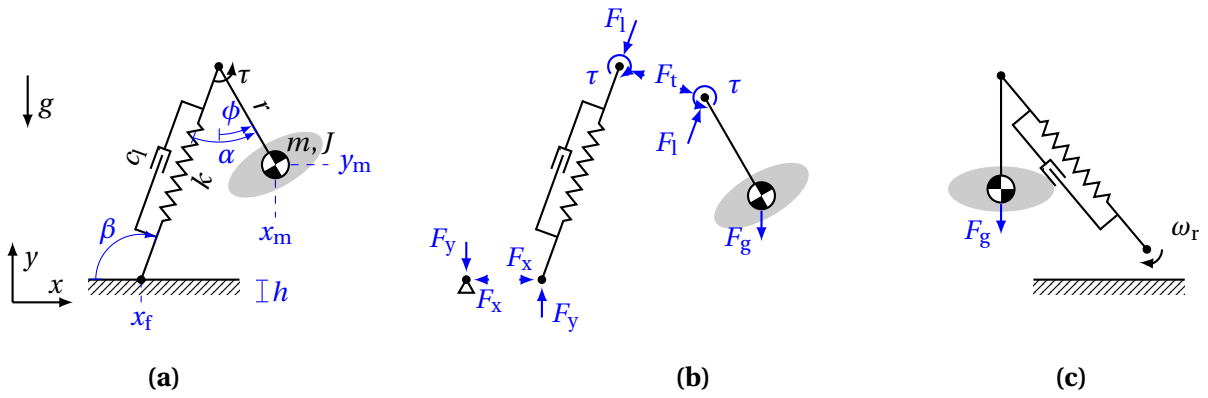

Figure 2.1: **(a)** Definition of the planar spring-mass model with a trunk (TSLIP) in stance phase. The body has mass m and rotational inertia J about the centre of mass. Its centre of mass is offset by a distance r from the hip joint. The Cartesian position of the centre of mass relative to the origin is given by its coordinates $(x_\mathrm{m}, y_\mathrm{m})$. The leg has a linear spring with stiffness k and resting length l_0, and damper with damping c_l. The leg and foot are massless. The foot is in contact with the ground at a height h. **(b)** The free-body diagram indicates the relevant force and torque definitions for the TSLIP model in stance. The vertical and horizontal ground reaction forces, F_y and F_x, apply at the foot. The compressive leg force F_l acts along the direction of the leg, F_t acts perpendicular to the leg at the hip. The extension torque τ is applied at the hip between the leg and the body. The force from gravitational acceleration F_g applies at the centre of mass. **(c)** Definition of the TSLIP model during the flight phase. The coordinate definitions are the same as during the stance phase. The only applied force is from the gravitational acceleration. The leg is retracted with a constant angular velocity ω_r with respect to the body.

and $\boldsymbol{C}$ is the vector with convective accelerations transformed to minimal coordinates,

$$\boldsymbol{C} = \begin{bmatrix} mr\dot{\phi}^2 \sin(\beta+\phi) - ml\dot{\beta}^2 \\ mrl\dot{\phi}^2 \cos(\beta+\phi) + 2ml\dot{\beta}\dot{l} \\ mrl\dot{\beta}^2 \cos(\beta+\phi) + 2mr\dot{\beta}\dot{l}\sin(\beta+\phi) \end{bmatrix}.$$

The full derivation of the equations of motion is provided in Appendix A.

The ground reaction forces follow from the balance of forces and moments on the leg,

$$F_\mathrm{x} = -F_\mathrm{l}\cos(\beta) + (\tau/l)\sin(\beta), \tag{2.5}$$

$$F_\mathrm{y} = F_\mathrm{l}\sin(\beta) + (\tau/l)\cos(\beta), \tag{2.6}$$

where F_x and F_y are the x and y components of the ground reaction force.

The flight phase is a purely ballistic motion illustrated in Figure 2.1 (c) which, in the absence of drag and applied forces, reduces the equations of motion to

$$m\ddot{y}_\mathrm{m} = -mg, \tag{2.7}$$

where $\ddot{y}_\mathrm{m}$ is the vertical acceleration of the centre of mass. All the other acceleration values equal zero.

2.3. Events

2.3.1. Stride Definition

The start of a stride occurs immediately following a touch-down. A succesful stride then has lift-off followed by another touch-down. The stride is considered unsuccessful if the model falls.

2.3.2. Lift-Off

The state transition from stance to flight occurs when the vertical ground reaction force calculated using Equation (2.6) equals zero,

$$F_{\mathrm{y}} = 0\,. \tag{2.8}$$

Upon lift-off the leg is reset to a reference hip angle α_{r} and reference angular velocity $\dot{\alpha} = -\omega_{\mathrm{r}}$, both with respect to local trunk coordinates. The reference angle is set such that for the periodic gait, touch-down occurs with the nominal touch-down angle β_0.

2.3.3. Touch-Down

The transition from flight to stance occurs when the foot is at ground height, h,

$$y_{\mathrm{m}} + r\cos(\phi) - l\sin(\beta) = h\,. \tag{2.9}$$

Impact of the foot is assumed to be perfectly inelastic and the foot is assumed not to slip. The inclusion of impact equations is not necessary because the leg and foot are massless.

2.3.4. Fall Detection

The model is assumed to fall when the centre of mass moves in the negative x direction,

$$\dot{x}_{\mathrm{m}} < 0\,, \tag{2.10}$$

or the hip point crosses the height of the ground reference,

$$y_{\mathrm{m}} + r\cos(\phi) \leq h\,. \tag{2.11}$$

The centre of mass reaching ground level ($y_{\mathrm{m}} = h$) is deliberately not chosen to cause a fall to allow us to evaluate the effects of the mass offset approaching the resting leg length.

2.4. Stance-Phase Control

We consider four stance-phase control strategies, the first of which is passive running,

$$\tau = 0\,. \tag{2.12}$$

The second stance-phase controller is a global proportional-derivative (PD) controller to represent a conventional control approach by controlling body pitch based on inertial measurements,

$$\tau = K_{\mathrm{p}}(\phi_{\mathrm{r}} - \phi) + K_{\mathrm{d}}(\dot{\phi}_{\mathrm{r}} - \dot{\phi})\,, \tag{2.13}$$

where ϕ_{r} and $\dot{\phi}_{\mathrm{r}}$ are the reference body pitch angle and angular velocity and $K_{\mathrm{p}} \geq 0$ and $K_{\mathrm{d}} \geq 0$ are the PD gains.

The third controller provides a simple model of an electrical motor driving the hip with a constant reference voltage. The body-pitch stability is left to passive dynamics and the controller is applied solely to the local angular velocity at the hip,

$$\tau = K_{\mathrm{d}}(\dot{\alpha}_{\mathrm{r}} - \dot{\alpha})\,, \tag{2.14}$$

where $\dot{\alpha}_{\mathrm{r}}$ is the reference hip angular velocity and $K_{\mathrm{d}} \geq 0$ is the derivative gain. This becomes a controller for global velocity assuming that pitch is also stabilized due to the predictable interaction between the leg and the ground in stance (Neville et al., 2006).

The fourth controller is a constant driving torque τ_c, which is used to evaluate the addition of damping in the leg,

$$\tau = \tau_c \,, \tag{2.15}$$

or with added damping at the hip,

$$\tau = \tau_c - c_h \dot{\alpha} \,, \tag{2.16}$$

with hip damping constant c_h. The local velocity controller is equivalent to a constant torque with hip damping where $\tau_c = K_d \dot{\alpha}_r$ and $c_h = K_d$.

If no damping is applied, the model with a constant driving torque reduces to the passive running model as described in Equation (2.12) because conservation of energy then requires the torque to be zero for the periodic gait.

2.5. Swing-Leg Retraction in Flight

Applying an angular retraction rate to the leg in the flight phase, starting from the apex of the centre of mass trajectory, has been shown to benefit stability in the SLIP model (Seyfarth, 2003). A swing-leg retraction strategy is applied to the TSLIP model to evaluate the possible contributions to stability and robustness. Measurement of the apex event may not be simple in experimental running (Karssen et al., 2015), so the swing-leg retraction is started with the instant leg reset upon lift-off.

The swing-leg retraction is locally defined and starts from lift-off at the reset angle α_r with a constant retraction rate ω_r,

$$\alpha(t) = \alpha_r - \omega_r (t - t_{LO}) \,, \tag{2.17}$$

where t_{LO} is the time of the last lift-off.

The swing-leg retraction rate can be normalized to $\bar{\omega}_r$ by centre of mass velocity v_0 and resting leg length l_0, such that the foot velocity is zero with respect to the ground for $\bar{\omega}_r = 1$,

$$\bar{\omega}_r = \frac{\omega_r l_0}{v_0} \,. \tag{2.18}$$

2.6. Base Parameter Choice

The simulation study is based on the TSLIP configuration in Table 2.1. The default configuration is the passive model. The other control strategies are applied as required for testing the hypotheses.

2.7. Numerical Integration

The equations of motion are numerically integrated with a Dormand-Prince 5(4) embedded Runge-Kutta integrator (Dormand and Prince, 1980) in Java, as implemented in Apache Commons Math 3.6. Absolute and relative tolerance on the integrated state are set to 1.0×10^{-8} in dimensionless units as per Table 3.1. The touch-down and lift-off events are implemented as switching conditions.

2.8. Finding Stable Limit Cycles

Periodic limit cycles are found by numerical optimization. A Covariant Matrix Adaptation Evolution Strategy (CMAES) (Hansen et al., 2009) is applied to minimize the cost function, imple-

Table 2.1: TSLIP model parameters for analysis. Parameters marked “opt.” are free in the optimization.

Parameter		Value	Unit
Passive			
Initial velocity	v_0	5.0	$\mathrm{g}^{1/2}\,\mathrm{L}^{1/2}$
Inertia	J	0.1	$\mathrm{M}\,\mathrm{L}^2$
Mass	m	1.0	M
Mass offset from hip	r	0.3	L
Gravitational acceleration	g	1.0	g
Leg stiffness	k	25.0	$\mathrm{M}\,\mathrm{g}\,\mathrm{L}^{-1}$
Touch-down angle	β_0	1.05	rad
Swing-leg retraction rate	ω_r	1.0	$\mathrm{rad}\,\mathrm{g}^{1/2}\,\mathrm{L}^{-1/2}$
Global PD controller			
Proportional gain	K_p	5.0	$\mathrm{M}\,\mathrm{g}\,\mathrm{L}\,\mathrm{rad}^{-1}$
Derivative gain	K_d	0.5	$\mathrm{M}\,\mathrm{g}^{1/2}\,\mathrm{L}^{3/2}\,\mathrm{rad}^{-1}$
Reference pitch angle	ϕ_r	0.0	rad
Reference pitch angular velocity	$\dot{\phi}_\mathrm{r}$	0.0	$\mathrm{rad}\,\mathrm{g}^{1/2}\,\mathrm{L}^{-1/2}$
Local velocity controller			
Derivative gain	K_d	0.5	$\mathrm{M}\,\mathrm{g}^{1/2}\,\mathrm{L}^{3/2}\,\mathrm{rad}^{-1}$
Reference hip angular velocity	$\dot{\alpha}_\mathrm{r}$	opt.	$\mathrm{rad}\,\mathrm{g}^{1/2}\,\mathrm{L}^{-1/2}$
Constant driving torque			
Leg damping coefficient	c_l	0.5	$\mathrm{M}\,\mathrm{g}^{1/2}\,\mathrm{L}^{-1/2}$
Torque constant	τ_c	opt.	$\mathrm{M}\,\mathrm{g}\,\mathrm{L}$

mented with the Apache Commons Math 3.6 library in Java. This is a stochastic method that does not require gradient information.

We combine the complete system configuration, $\boldsymbol{x}$, and velocities, $\dot{\boldsymbol{x}}$, into the state vector $\boldsymbol{z}$. The horizontal position x_m is not periodic and therefore the first element is removed from the state vector. The cost function $C_1(\boldsymbol{z})$ for finding a fixed point takes the sum of squared differences over one step,

$$\boldsymbol{z} = \begin{bmatrix} \boldsymbol{x} \\ \dot{\boldsymbol{x}} \end{bmatrix}, \tag{2.19}$$

$$C_1(\boldsymbol{z}) = (\boldsymbol{z}_n - \boldsymbol{z}_{n+1})^\mathrm{T}(\boldsymbol{z}_n - \boldsymbol{z}_{n+1}). \tag{2.20}$$

The initial state $\boldsymbol{z}_n$ is set to always start at the beginning of the stance phase with the foot on the ground. The state after one step $\boldsymbol{z}_{n+1}$ is the result of numerically integrating a full step and taking the system state immediately after touch-down.

If the value of the first cost function, $C_1(\boldsymbol{z})$, is smaller than a threshold $\epsilon = 1 \times 10^{-4}$, the optimization switches to the second cost function $C_2(\boldsymbol{q}^*)$, which takes the state at the fixed point and returns the square of the largest eigenvalue that has magnitude not equal to one,

$$C_2(\boldsymbol{q}^*) = \max|\lambda_i|^2, \qquad |\lambda_i| \neq 1, \qquad i \in [0,2] \tag{2.21}$$

The first cost function is offset by a constant value of 25, such that it is always larger than the second cost function for the largest eigenvalue smaller than 5.

The complete optimization problem is to minimize the combined cost function $C(\boldsymbol{a},\boldsymbol{p})$, which takes the vector with free initial conditions $\boldsymbol{a}$ and vector with free configuration parameters $\boldsymbol{p}$, both subject to lower and upper bounds per variable,

$$\min_{\boldsymbol{a},\boldsymbol{p}} \quad C(\boldsymbol{a},\boldsymbol{p}) \begin{cases} C_1(\boldsymbol{z}) + 25 & \text{if } C_1(\boldsymbol{z}) > \epsilon, \\ C_2(\boldsymbol{q}^*) & \text{otherwise,} \end{cases} \tag{2.22}$$

$$\text{s.t.} \quad \boldsymbol{a}_\mathrm{l} \leq \boldsymbol{a} \leq \boldsymbol{a}_\mathrm{u}, \tag{2.23}$$

$$\boldsymbol{p}_\mathrm{l} \leq \boldsymbol{p} \leq \boldsymbol{p}_\mathrm{u}. \tag{2.24}$$

The free initial conditions are the angle between the velocity vector and the horizontal axis δ, the body pitch ϕ, body pitch rate $\dot{\phi}$, and the leg reset angle α_r.

3

Methods for Simulation Study

3.1. Outcome Measures

3.1.1. Dimensional Analysis

All units are normalized by body mass M, gravitational acceleration g, and resting leg length L (McMahon and Bonner, 1983; McMahon and Cheng, 1990). The resulting scaling factors are listed in Table 3.1. The normalized parameters are calculated by division with the scaling factor,

$$\text{normalized quantity} = \frac{\text{quantity in SI units}}{\text{scaling factor}}. \tag{3.1}$$

Table 3.1: Dimensional analysis and scaling factors.

Quantity (SI unit)	Dimensions	Scaling factor
Length (m)	[L]	L
Time (s)	[T]	$g^{-1/2} L^{1/2}$
Frequency (Hz)	[T^{-1}]	$g^{1/2} L^{-1/2}$
Position (m)	[L]	L
Speed (m s^{-1})	[L T^{-1}]	$g^{1/2} L^{1/2}$
Acceleration (m s^{-2})	[L T^{-2}]	g
Mass (kg)	[M]	M
Inertia (kg m^2)	[M L^2]	M L^2
Force (N)	[F]	M g
Torque (N m)	[F L]	M g L
Impulse (N s)	[F T]	M $g^{1/2} L^{1/2}$
Stiffness (N m^{-1})	[F L^{-1}]	M g L^{-1}
Damping (N s m^{-1})	[F L^{-1} T]	M $g^{1/2} L^{-1/2}$
Energy (J)	[F L]	M g L

3.1.2. Stability of the Periodic Gait

In this work we define stability as the response of the periodic limit cycle of the gait to small perturbations, as was applied for passive running by McGeer (1990). The orbital stability of

the limit cycle is evaluated using the Floquet multipliers, which are the eigenvalues of the Jacobian of the linearized stride-to-stride map (Parker and Chua, 1989). The calculation of the eigenvalues is described in Appendix B.

We define $\boldsymbol{q}_n$ as the state vector at the Poincaré section of step n, with the Poincaré section taken just after touch-down. The gait has a periodic limit cycle, or fixed point, when the state at the Poincaré section does not change from step to step,

$$\boldsymbol{q}_n = \boldsymbol{q}_{n+1} = \boldsymbol{q}^* , \tag{3.2}$$

where $\boldsymbol{q}^*$ is the system state at the fixed point. We consider only gaits that are single-step periodic, even though multi-step stable gaits may exist where $\boldsymbol{q}_n = \boldsymbol{q}_{n+i}$ for $i > 1$.

The limit cycle is asymptotically stable if the magnitudes of all eigenvalues are smaller than one. Eigenvalue magnitudes equal to one indicate neutral stability; these are present if the dynamic system has a conservative nature. Neutral stability is considered sufficient for a stable running gait in the domain of this study. The limit cycle is considered unstable if the magnitude of any eigenvalue is larger than one.

3.1.3. Robustness to Large Disturbances

We define robustness as the resistance to falling. It is measured by taking the largest disturbance from the periodic limit cycle which does not result in a fall within 25 steps. The robustness limits are found with a binary search method over the following variables:

1. Step-down (Δh),
2. Horizontal velocity ($\Delta \dot{x}_\mathrm{m}$),
3. Pitch rate ($\Delta \dot{\phi}$).

Robustness is only computed for limit cycles that are at least neutrally stable.

3.2. Mechanism for Pitch Stabilization

Metacentric stability principles such as the virtual pivot point (Maus et al., 2008, 2010) depend on location and the direction of the ground reaction forces. To investigate whether metacentric stabilization may explain pitch stability, the ground reaction force vector $\boldsymbol{F}$ is integrated for each step to a single ground reaction impulse $\boldsymbol{I}$,

$$\boldsymbol{I} = \int_{t_0}^{t_1} \boldsymbol{F} \mathrm{d}t , \tag{3.3}$$

where t_0 is the touch-down time and t_1 is the lift-off time. The ground reaction impulse is linearized with respect to a pitch disturbance from the limit cycle,

$$\boldsymbol{I} \approx \boldsymbol{I}(\boldsymbol{q}^*) + \frac{\partial \boldsymbol{I}}{\partial \boldsymbol{q}} \Delta \boldsymbol{q} , \tag{3.4}$$

where $\boldsymbol{q}^*$ is the state at the fixed point and $\Delta \boldsymbol{q}$ is the disturbance from the fixed point. The point of application of the impulse $(x_\mathrm{p}, y_\mathrm{p})$ is determined relative to centre of mass by

$$x_\mathrm{p} = \frac{\int x F_\mathrm{y} \mathrm{d}t}{\int F_\mathrm{y} \mathrm{d}t}, \qquad y_\mathrm{p} = \frac{\int y F_\mathrm{x} \mathrm{d}t}{\int F_\mathrm{x} \mathrm{d}t} . \tag{3.5}$$

The response of the resultant ground impulse is evaluated over varying pitch disturbance and linearized about the neutral point.

The observed impulse and ground reaction forces are plotted to enable the comparison to the hanging pendulum for stability. We compare the passive TSLIP response to the global PD-controlled response to see whether the virtual pendulum concept is still applicable.

3.3. Undamped Height and Velocity Stability

The passive TSLIP model is a conservative system. Following a change in ground height Δh, the change in potential energy ΔE_p leads to a change in kinetic energy ΔE_k. Assume that the apex height in flight converges to the same steady-state height above the ground and the rotational element in kinetic energy is negligibly small. All potential energy is then converted to kinetic energy,

$$\Delta E_\mathrm{p} = mg\Delta h = -\Delta E_\mathrm{k}\,, \tag{3.6}$$

$$\Delta E_\mathrm{k} = \frac{1}{2}m\left(v_\infty^2 - v_0^2\right) = -mg\Delta h\,, \tag{3.7}$$

where v_0 is the initial centre-of-mass velocity at touch-down and v_∞ is the final velocity of the centre of mass at touch-down when the system has reached a steady state. The theoretical total change in velocity Δv is then

$$\Delta v = v_\infty - v_0 = -v_0 + \sqrt{v_0^2 - 2\Delta h}\,. \tag{3.8}$$

We subject the passive TSLIP model to a 0.2 L step-down change in ground height. The height and velocity of the centre of mass are observed to establish convergence to a steady state.

For the passive model and the local-velocity-controlled model, we record the final velocity following a step change in ground-height disturbance and compare these to the theoretical expected values.

We expect the angle of the velocity vector at touch-down to to contribute to the stabilization of height and velocity by influencing the stance-phase behaviour. We test for the stabilizing mechanism by setting the model at the start of a stride and adjusting the angle of the velocity vector from the periodic gait.

3.4. Running Velocity

3.4.1. Velocity Variation

For an evaluation of the impact of velocity on stability and robustness, we take the passive TSLIP model with the configuration in Table 2.1. The initial velocity is then varied in the range $v_0 \in [1,10]\mathrm{g}^{1/2}\,\mathrm{L}^{1/2}$.

3.4.2. Parameter Space

Self-stable gaits for the SLIP model depend on choosing a suitable combination of leg stiffness and touch-down angle (Seyfarth et al., 2002). We hypothesize that increasing running velocity reduces the sensitivity to parameter changes for self-stable gaits, specifically considering leg stiffness and touch-down angle. A grid search for stable gaits is performed over varying leg stiffness and touch-down angle, for a normalized velocity $v_0 \in [2,3,4,5]\mathrm{g}^{1/2}\,\mathrm{L}^{1/2}$.

3.4.3. Stride Properties

At low speeds, the stance duration t_s is dominated by the bounce duration t_b of the spring-mass system, which is half of a full period of oscillation,

$$t_b = \pi\sqrt{\frac{m}{k}}. \tag{3.9}$$

This does not apply at higher speeds where the stance phase becomes determined by velocity and leg touch-down angle, instead of stiffness and bounce duration,

$$t_s \approx \frac{2l_0(\pi/2-\beta_0)}{v_0}. \tag{3.10}$$

The flight duration t_f is related to velocity v_0 and the angle δ between the velocity vector and the horizontal axis,

$$t_f = \frac{2\dot{y}_m}{g} \approx \frac{2v_0\delta}{g}. \tag{3.11}$$

The ratio between spring-mass bounce duration and velocity-based swing duration, which we refer to as the fast-running index I_{fr}, can be used to discern between fast and slow running,

$$I_{fr} = \frac{t_b}{t_s} = \frac{\pi v_0\sqrt{m/k}}{l_0(\pi-2\beta_0)}. \tag{3.12}$$

For $I_{fr} = 1$, the bounce and swing duration are equal, indicating a centre-of-mass trajectory with a large vertical change. This trajectory becomes more horizontal for increasing speeds. We define fast running for approximately $I_{fr} > 2$. At low I_{fr}, foot placement and running speed are tightly coupled. This coupling is reduced for higher values of the fast-running index.

3.5. Damping in the Leg or Hip

Addition of dissipative elements may increase stability over the undamped response. Both damping in the leg and in the hip may contribute to stabilization of the running gait.

We consider the TSLIP model with a constant driving torque for simplicity. The stability and robustness measures are then evaluated separately for varying leg damping ($c_l \in [0,3]$) and varying hip damping ($c_h \in [0,3]$), where the constant torque is the result of the optimization such that it balances the energy dissipated in the damper for stable periodic running at the given initial velocity v_0.

3.6. Parameter Variation

3.6.1. Mass Offset

We expect the passive model to be stable for a mass below the hip due to metacentric pitch stability. The discrete nature of the running system is likely to cause instability in pitch if the mass offset becomes too large. The stability and robustness measures are evaluated for the mass offset $r \in [-1,1]$L.

3.6.2. Leg Stiffness

The effects on stability and robustness of changing leg stiffness for the TSLIP model is evaluated for $k \in [0, 200]\mathrm{M\,g\,L^{-1}}$. Stiffer legs are expected to better support the centre of mass after a step-down change in ground height and are therefore likely to be more robust to step-down disturbance. However, we expect legs that are too stiff to results in poor robustness due to smaller acceptable deviations from the periodic gait for stable running.

3.6.3. Touch-Down Angle

We measure the stability and robustness measures for the touch-down angle $\beta_0 \in [0.8, 1.5]\mathrm{rad}$. For a fixed leg stiffness and swing-leg retraction rate, flatter touch-down angles are expected to perform better in step-down robustness because they allow for a larger step-down without missing the stance phase.

3.6.4. Swing-Leg Retraction

A swing-leg retraction strategy is applied to the TSLIP model to evaluate the possible contributions to stability and robustness on a range of normalized retraction rates $\bar{\omega}_r \in [0, 2]$.

3.7. Control Strategy Comparison

The performance for the different control strategies is expected to differ primarily in their response over varying mass offset from the hip. The stability and robustness measures for the different control strategies are therefore compared for mass offset $r \in [-1, 1]\mathrm{L}$. We expect that the control at the hip should not be significantly affected by differing leg stiffness, touch-down angle, or retraction rate.

4

Simulation Results

4.1. Response to Pitch Disturbance

In response to a pitch disturbance, the ground impulse response changes as illustrated in Figure 4.1. For small disturbances, the linearized gradients are approximately zero for all except the horizontal position with respect to the centre of mass. This horizontal movement of the ground reaction impulse results in a torque about the centre of mass that counteracts the pitch disturbance. The direction and size of the impulse remain constant for small disturbances. This change in position of the resultant ground impulse with respect to the centre of mass is

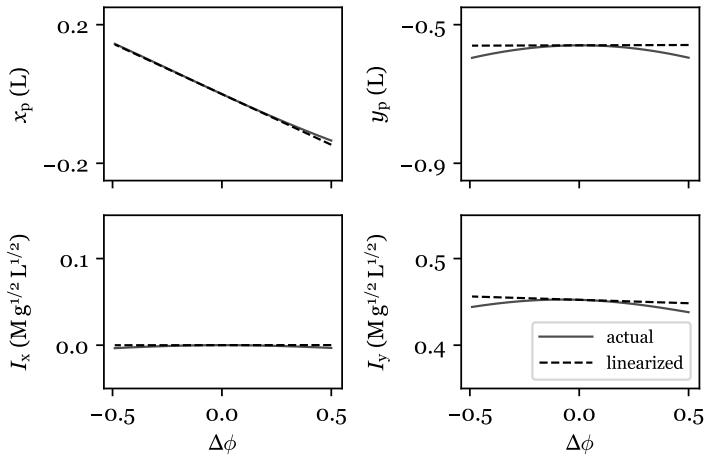

Figure 4.1: Linearization of the ground impulse response to pitch disturbance. x_p and y_p are the point of application of the impulse with respect to the centre of mass (Equation (3.5)). I_x and I_y are the x and y components of the resultant ground impulse $\boldsymbol{I}$ (Equation (3.3)). The TSLIP model is passive, with the full configuration listed in Table 2.1. The steepest gradient is in the horizontal position of the ground impulse with respect to the centre of mass, indicating a shift to provide a restoring torque.

illustrated in Figure 4.2 for both a negative and a positive change in pitch angle. The position of the ground impulse remains below the hip and the direction does not change.

The PD-controlled response to a pitch disturbance is illustrated in Figure 4.3. The position with respect to the centre of mass of the resultant ground impulse remains unchanged as pitch

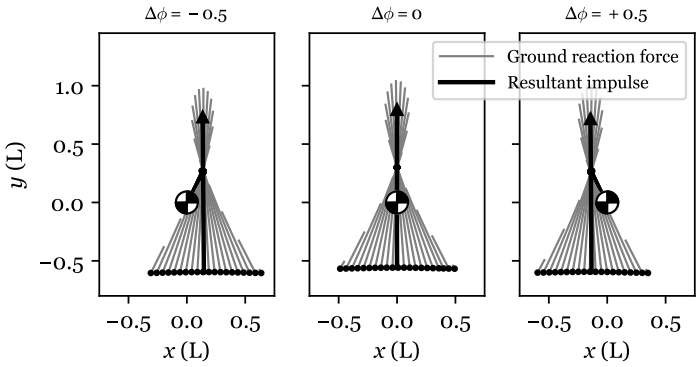

Figure 4.2: The TSLIP model is perturbed in its body pitch from the stable periodic limit cycle. All coordinates are taken with respect to the centre of mass. The model configuration is listed in Table 2.1. The direction of the ground reaction forces is shown as well as the resultant ground impulse. The impulse remains approximately directed towards the hip, which causes a torque about the centre of mass opposite to the pitch disturbance, indicating the metacentric pitch stability.

is perturbed. However, the correcting torque applied at the hip by the PD controller results in a large change in direction of the ground impulse.

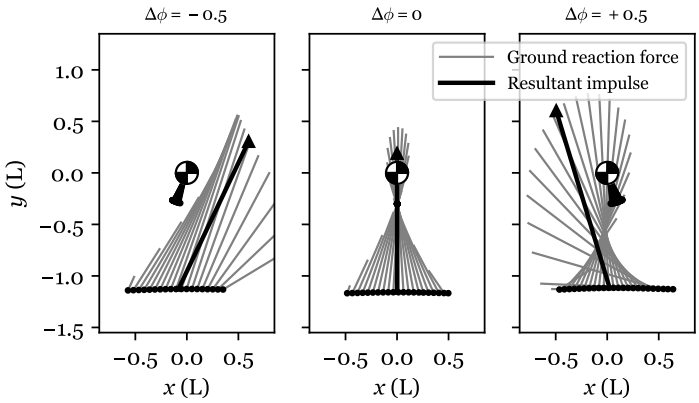

Figure 4.3: The TSLIP model with a global PD controller on body pitch is shown. The mass above the hip is perturbed in its body pitch from the stable periodic limit cycle. All coordinates are taken with respect to the centre of mass. The model configuration is listed in Table 2.1. The direction of the ground reaction forces is shown as well as the resultant ground impulse. The impulse position remains below the hip. The direction is changed because of the hip torque that the controller applies to restore the body pitch, which does not resemble metacentric pitch stabilization.

4.2. Undamped Height and Velocity Stability

The passive TSLIP model converges to the expected velocity from the energy balance in Equation (3.8), as illustrated in Figure 4.4 (left). The model with a local velocity controller converges back to the initial velocity as shown in Figure 4.4 (right).

The behaviour of the velocity and height of the centre of mass after a 0.2 L step-down disturbance is illustrated in Figure 4.5. The system stabilizes with a multi-step oscillation, as is also visible in Figure 4.6 which shows the trajectory of the centre of mass and the body configuration at touch-down. Height and horizontal velocity oscillate in opposite phase.

A step disturbance in ground height changes the direction of the velocity vector at touch-

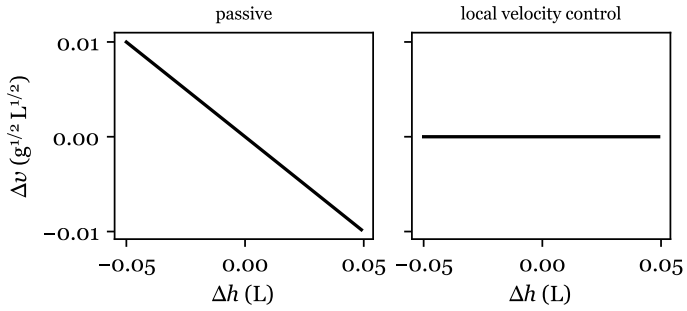

Figure 4.4: Change in velocity with respect to initial velocity of 5 $g^{1/2} L^{1/2}$ after a step change in ground height, measured after the gait has converged to a steady state., The passive model converges to a velocity change as expected from Equation (3.8). When the local velocity controller is applied, the gait converges back to the initial velocity.

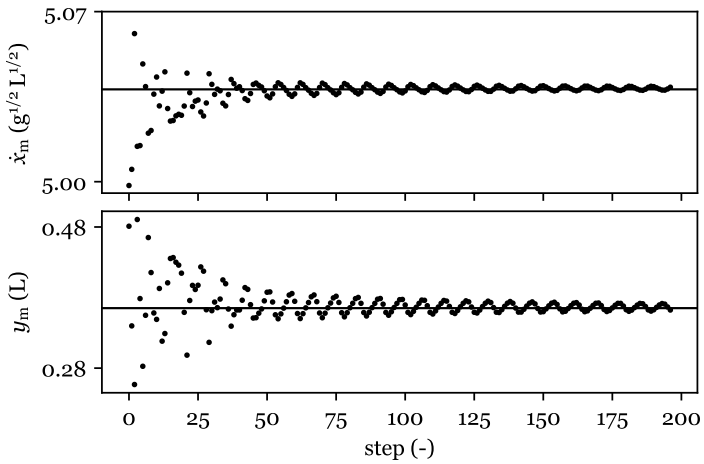

Figure 4.5: Horizontal velocity and height of the centre of mass after a 0.2 L step-down disturbance; the data marks the values at touch-down for each step. Velocity and height oscillate in opposite phase and converge towards a steady state. The simulation uses the passive TSLIP model with configuration listed in Table 2.1.

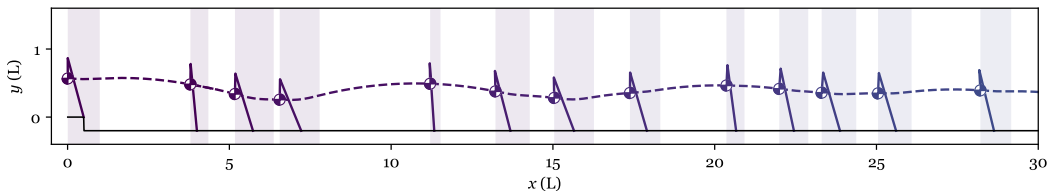

Figure 4.6: Trajectory of the centre of mass and model configuration drawn at touch-down per step, after a 0.2 L step-down disturbance; the shaded areas indicate the stance phase. Passive model with configuration listed in Table 2.1. The trajectory of the centre of mass shows a multi-step oscillation converging back to the single-step periodic gait. The touch-down leg angle changes each step due to the combination of a constant retraction rate and differing flight times.

down with respect to the periodic gait. This has an effect on the stance phase behaviour that is illustrated in Figure 4.7 (top). Landing with a larger downward vertical velocity component, i.e. after a step-down, leads to a longer stance phase and a flatter lift-off trajectory than in the periodic gait. Subsequently, the flight phase is shorter. Conversely, if the vertical velocity component is adjusted upwards, i.e. a step-up, the stance phase is shorter, with a steeper lift-off and longer flight phase.

The change in the ground reaction forces shows a larger vertical force for larger downward velocity as the spring is compressed more (Figure 4.7 (middle)). The magnitude of the horizontal ground reaction forces becomes asymmetric, such that the resultant ground impulse is directed forward after a step-down and backward after a step-up change in ground height (Figure 4.7 (bottom)). The net result is that excess downward vertical velocity at touch-down is converted into horizontal forward velocity.

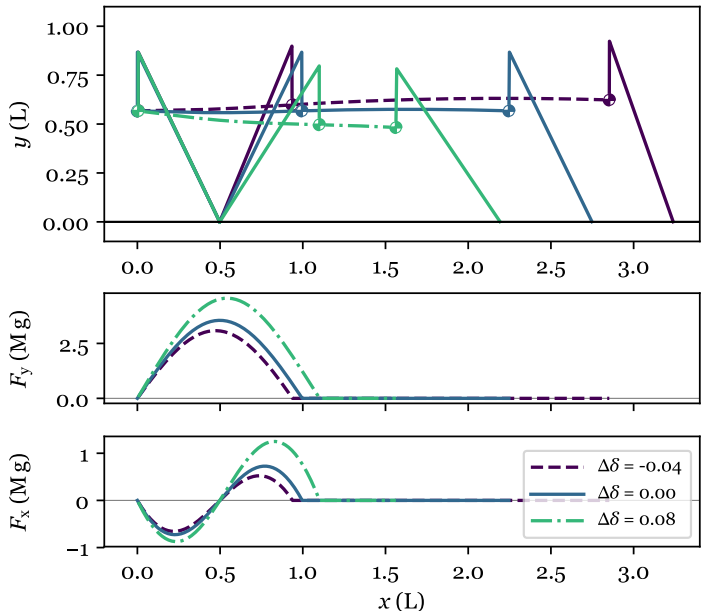

Figure 4.7: Illustration of the effect of changing the angle δ between the velocity vector of the centre of mass and the horizontal axis. The trajectory of the centre of mass is drawn for a single step with the TSLIP configuration drawn at touch-down, lift-off, and touch-down (top), with the related vertical (middle) and horizontal (bottom) components of the ground reaction forces. Passive model with configuration in Table 2.1. As the vertical velocity component is adjusted downward from the periodic gait, the time and distance covered in stance increases. The asymmetry in the ground reaction force converts excess vertical, downward velocity into horizontal, forward velocity.

4.3. Effects of Running Faster

4.3.1. Velocity Variation

Running is stable with the TSLIP model above a minimum velocity. The gaits converge most quickly per step for velocities just over the minimum velocity threshold for stable running as illustrated in Figure 4.8. At higher velocities there is little variation of convergence with speed.

The maximum step-down disturbance is velocity dependent as shown in Figure 4.9 (top). There is a peak in step-down robustness in this configuration for a normalized velocity around $4.0\,g^{1/2}\,L^{1/2}$ and around $5.0\,g^{1/2}\,L^{1/2}$. Further increase in velocity reduces the ability to handle

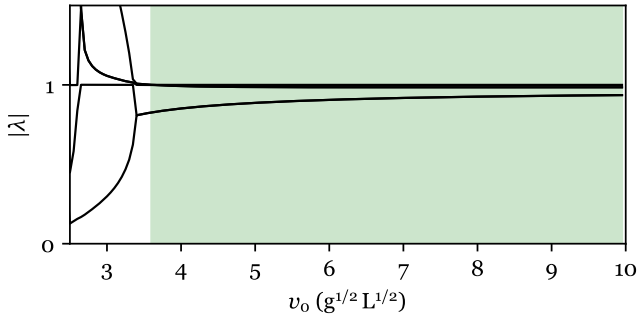

Figure 4.8: Eigenvalue magnitudes of the TSLIP model over varying velocity. Green areas mark the stable domain. Model configuration is passive as in Table 2.1. There is a minimum running velocity determined by the model configuration, increasing velocity reduces convergence per step.

a step-down disturbance.

The maximum horizontal push disturbance (Figure 4.9 (middle)) increases almost linearly with increasing velocity, such that the minimum velocity is constant for a fixed model configuration.

The robustness to pitch-rate disturbance varies only minimally with velocity (Figure 4.9 (bottom)).

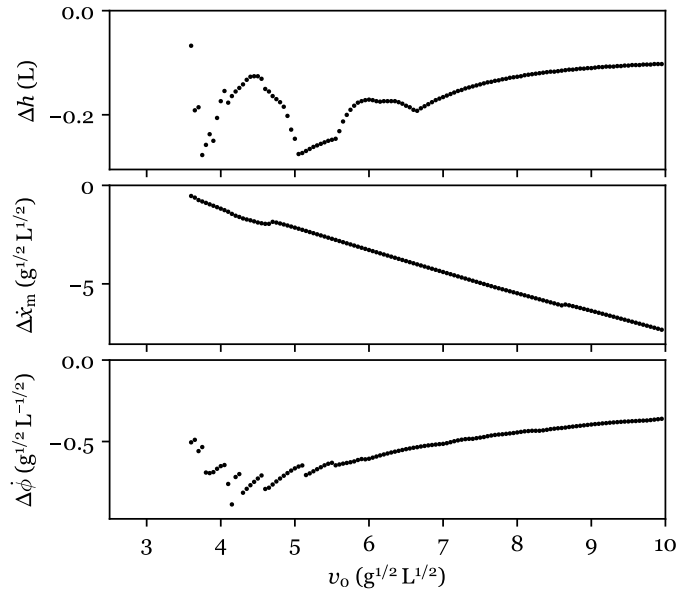

Figure 4.9: TSLIP robustness to step-down (top), horizontal push (middle), and pitch-rate disturbance (bottom) over varying initial velocity. Model configuration is passive as in Table 2.1. There is an optimum velocity for step-down robustness, further increasing velocity above that reduces the maximum step-down. The resistance to a push disturbance is primarily governed by the minimum speed for stable running for the specified configuration.

4.3.2. Parameter Space

The range of possible leg stiffness and touch-down angle combinations for which a stable gait can be found is larger for faster running as shown in Figure 4.10. The range of touch-down leg angles that allows self-stable running is wider for a given stiffness at a higher velocity.

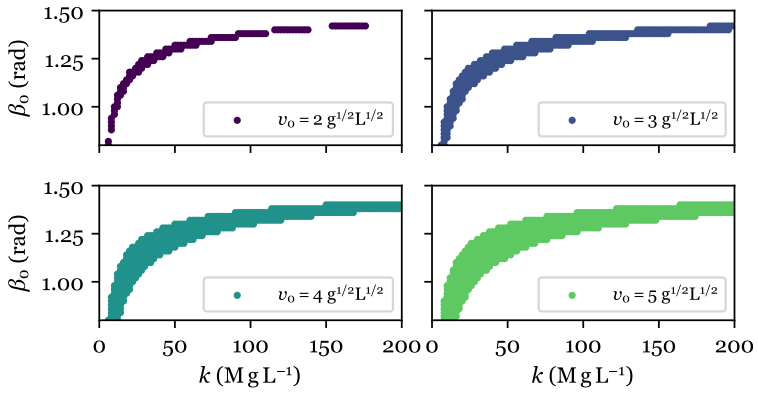

Figure 4.10: Illustration of the range of leg stiffness and touch-down angle combinations which yield stable periodic limit cycles. The TSLIP model is run with a local angular velocity controller and the configuration specified in Table 2.1. The range of configurations is larger for faster running, indicating foot placement and leg stiffness become less critical.

4.3.3. Stride Properties

Figure 4.11 illustrates the effect of initial velocity, leg stiffness, and initial leg angle on stance and flight time. Stance time is not affected by stiffness, decreases with increasing velocity and steeper initial leg angles. Flight time increases with increasing stiffness and decreases with increasing velocity and steeper initial leg angle. The values match closely to the theoretical expected values calculated with Equations (3.10) and (3.11).

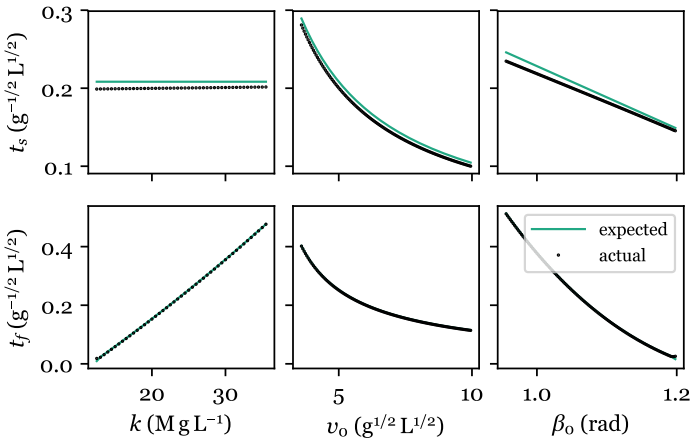

Figure 4.11: Stance and flight time over changing parameters compared to expected value. Passive TSLIP model, configuration as in Table 2.1. Expected values calculated using Equations (3.10) and (3.11) with the other variables constant.

4.4. Adding Damping

4.4.1. Damping in the Leg

The addition of leg damping improves stability as shown in Figure 4.12. Leg damping affects the stabilization of centre-of-mass height and velocity. The constant driving torque required for energetic equilibrium increases with increasing damping because it is tuned such that the power from actuation balances the dissipation in the damper.

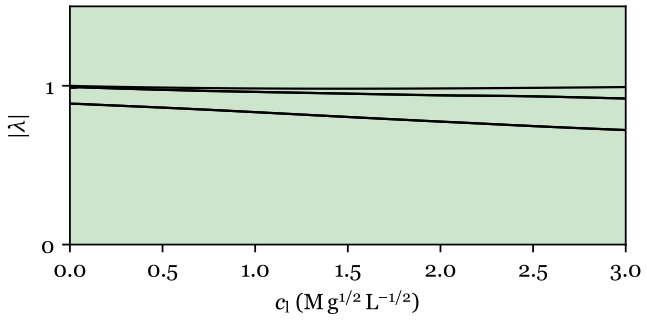

Figure 4.12: Eigenvalue magnitudes for the TSLIP model over varying leg damping with a constant driving torque controller. Stable domain is marked in green. Configuration as in Table 2.1. Damping in the leg improves height and velocity stability.

Leg damping has a negative effect on all of step-down, push, and pitch-rate robustness as illustrated in Figure 4.13. Increasing damping leads to lower stance durations and longer flight durations. This relates to an increased probability of missing a stance phase, causing the model to fall.

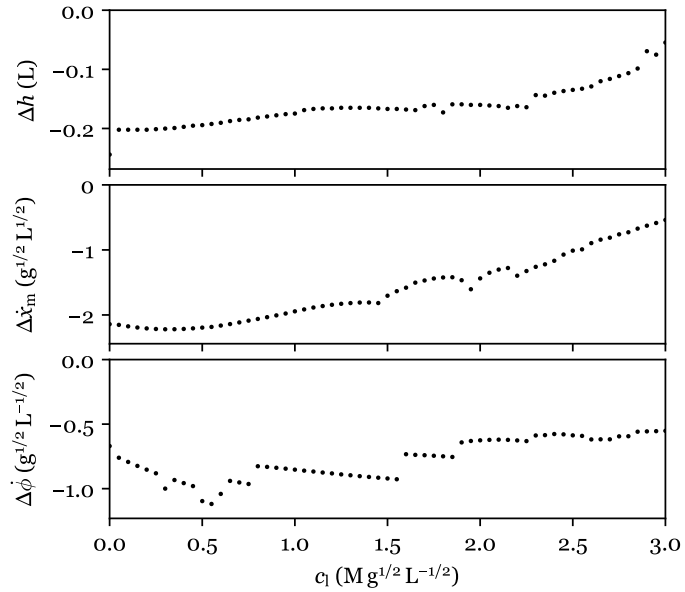

Figure 4.13: TSLIP robustness to step-down (top), horizontal push (middle), and pitch-rate disturbance (bottom) over varying leg damping for the model with a constant driving torque. Configuration as in Table 2.1. High damping in the leg negatively affects robustness to all of step-down, horizontal push, and pitch-rate disturbances.

4.4.2. Damping at the Hip

Hip damping positively affects the stability of the model in response to pitch and pitch-rate disturbances. The eigenvalues over varying hip damping are illustrated in Figure 4.14.

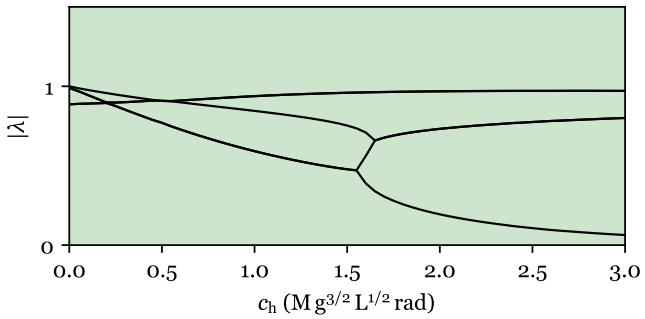

Figure 4.14: Eigenvalue magnitudes for the TSLIP model over varying hip damping with a constant driving torque. Stable domain is marked in green. Configuration as in Table 2.1. The addition of hip damping improves pitch stability, although this is not necessarily the most unstable mode.

Hip damping has only minimal influence on the robustness to step-down disturbance, illustrated in Figure 4.15 (top). It does not affect the stance and flight duration of the gait in the way leg damping does.

The angular velocity at the hip is related to the forward velocity in stance phase. The robustness to push disturbance decreases as hip damping increases as shown in Figure 4.15 (middle).

The addition of damping at the hip strongly improves the robustness to pitch-rate disturbance as shown in Figure 4.15 (bottom).

4.5. Parameter Variation

4.5.1. Mass Offset

Figure 4.16 illustrates the change in eigenvalues for a varying mass offset from the hip. The gait becomes stable for mass offset below the hip. The variation is small for a lower hanging mass, until the gait sharply becomes unstable for mass offset over 0.86 L.

The robust region is bounded by the mass-offset range for stable running as is shown in Figure 4.17. For this configuration, having a mass offset up to 0.5 L below the hip improves the robustness to a step-down disturbance as shown in Figure 4.17 (top). Further increasing the mass offset reduces robustness until the gait becomes unstable at $r \approx 0.86\,\mathrm{L}$.

There is little impact of mass offset on robustness to push disturbance (Figure 4.17 (middle)) as there is no coupling between the hanging mass and velocity for passive running.

Having a mass offset further from the hip improves resistance to a pitch-rate disturbance up until $r \approx 0.5\,\mathrm{L}$, illustrated in Figure 4.17 (bottom). Further increases in mass offset do not affect pitch-rate robustness until the robustness reduces for $r > 0.75\,\mathrm{L}$.

4.5.2. Stiffness

The stability improves for increasing stiffness, up to an upper limit where the fixed points become unstable, illustrated in Figure 4.18. No periodic limit cycles are found when the stiffness

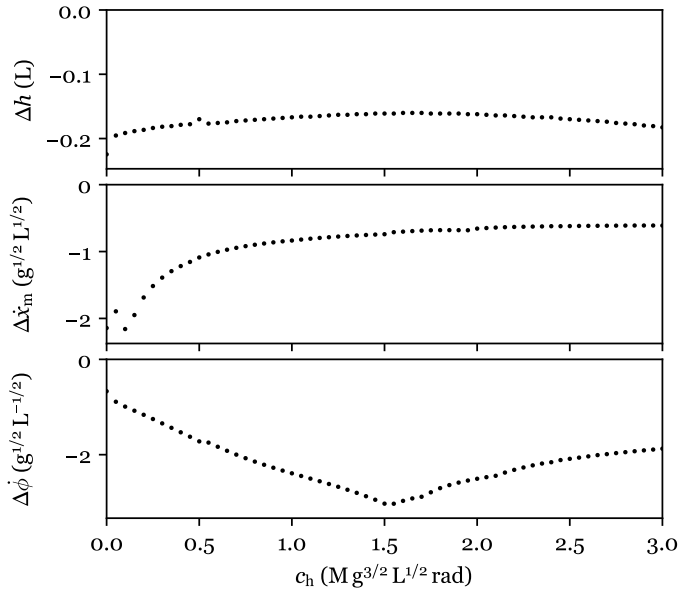

Figure 4.15: TSLIP robustness to step-down (top), horizontal push (middle), and pitch-rate disturbance (bottom) over varying damping at the hip with a constant driving torque. The model configuration is provided in Table 2.1. The addition of hip damping improves the robustness to a pitch-rate disturbance, but reduces the robustness to a change in horizontal velocity.

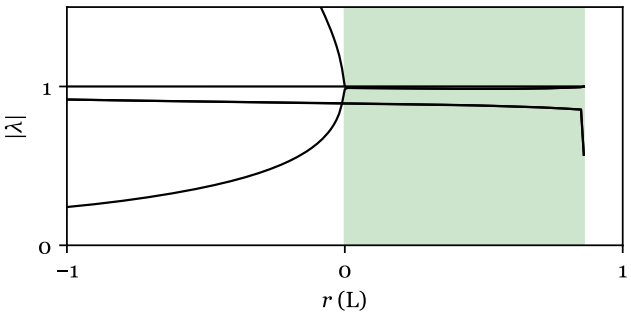

Figure 4.16: Eigenvalue magnitudes for the TSLIP model over varying mass offset. Stable domain is marked in green. Configuration is passive as in Table 2.1. Passive self-stable gaits exist for a mass offset below the hip.

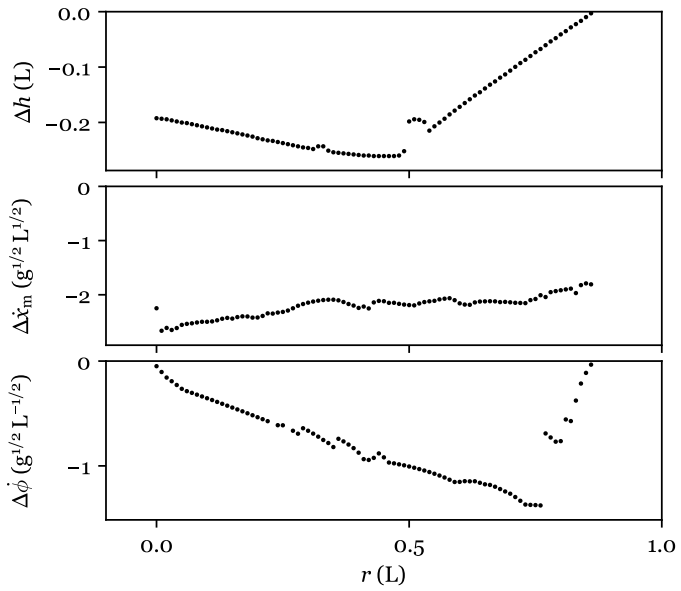

Figure 4.17: TSLIP robustness to step-down (top), horizontal push (middle), and pitch-rate disturbance (bottom) over varying mass offset. Model configuration in Table 2.1. Hanging-mass configurations exhibit robust behaviour without explicit inertial references. Increasing the mass offset has a positive effect on robustness for r smaller than 0.5 L.

is too low. On the contrary, if stiffness is increased above the upper limit for stable running, periodic running gaits are still found, even though they are unstable.

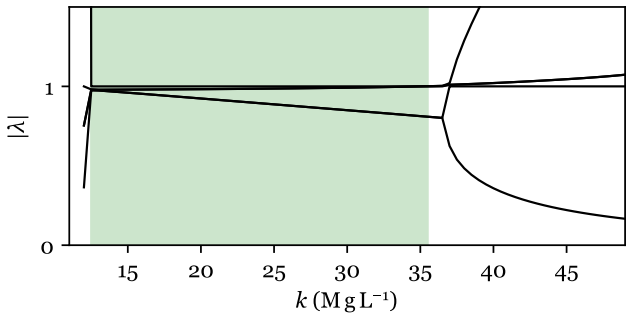

Figure 4.18: Eigenvalue magnitudes for the TSLIP model over varying leg stiffness. Stable domain is marked in green. Configuration is passive as in Table 2.1. There is a wide range of possible leg stiffness values for stable running gaits.

The maximum step-down increases for stiffer legs, as shown in Figure 4.19 (top), although the robustness decreases sharply above a certain threshold.

Figure 4.19 (middle) shows how the resistance to a push disturbance decreases for increasing stiffness. The push disturbance relates to the minimum required speed for stable running. Lower leg-stiffness values allow a larger push disturbance, which equates to a lower minimum velocity for stable running.

The optimum stiffness for handling a pitch-rate disturbance is in the middle of the stable range as shown in Figure 4.19 (bottom).

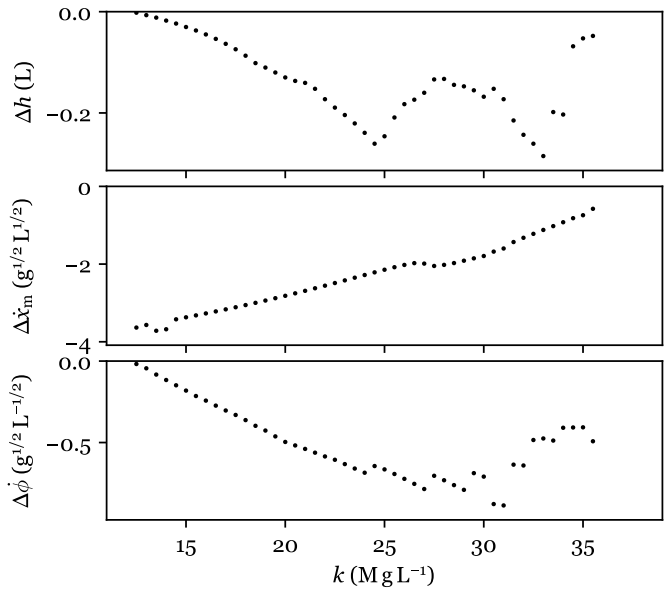

Figure 4.19: TSLIP robustness to step-down (top), horizontal-push (middle), and pitch-rate disturbance (bottom) over varying leg stiffness value. The model is passive with the configuration as in Table 2.1. Stiffer legs up to the mid range tend to be more robust to a step-down disturbance. More compliant legs are able to handle a push disturbance better as they allow a lower minimum running speed. A leg stiffness in the middle of the stable range is best for robustness to pitch-rate variation.

4.5.3. Touch-Down Angle

Leg angle and stiffness appear to be coupled for stable running, visualized in Figure 4.10. Lower stiffness requires flatter initial leg angles. Vice-versa, higher stiffness requires steeper initial leg angles.

Flatter leg angles demonstrate better stability within the stable range shown in Figure 4.20. The gait gradually becomes unstable if the leg angle becomes too flat, but periodic limit cycles still exist. No periodic limit cycles are found when the touch-down angle becomes too steep.

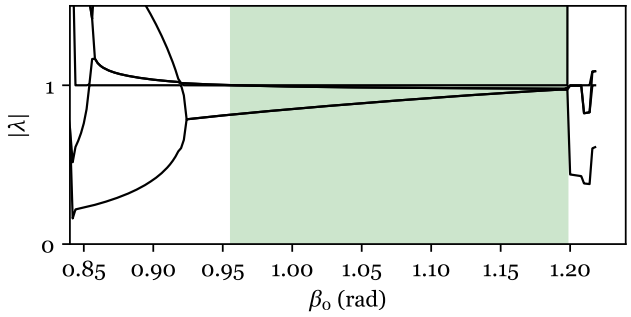

Figure 4.20: Eigenvalue magnitudes for the TSLIP model over varying initial leg angle. Stable domain is marked in green. Configuration is passive as in Table 2.1. There is a range of leg angles for stable running gaits.

Flatter leg angles perform better in response to step-down disturbance as shown in Figure 4.21 (top).

For push disturbance, illustrated in Figure 4.21 (middle), steeper leg angles provide large robustness. This indicates a lower minimum velocity for steeper leg angles.

The robustness to pitch-rate disturbance shown in Figure 4.21 (bottom) shows that the model is most robust in the middle of the range of touch-down angles for stable running.

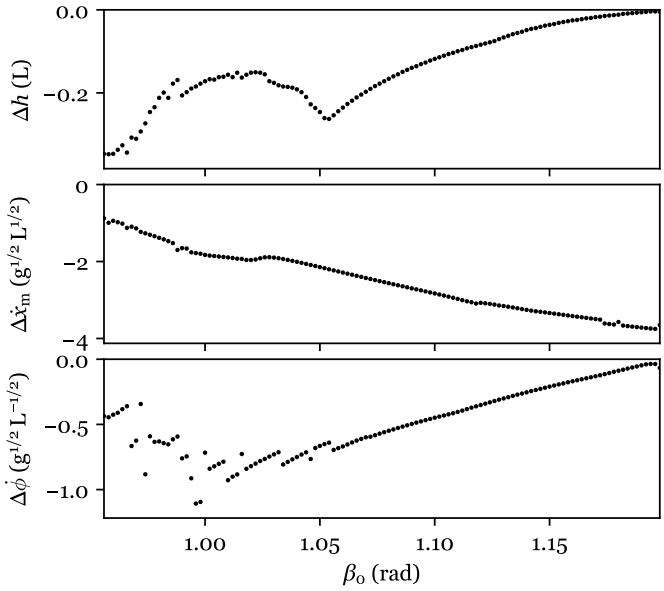

Figure 4.21: TSLIP robustness to step-down (top), horizontal push (middle), and pitch-rate disturbance (bottom) for the four different control strategies over varying leg touch-down angle. Configuration as in Table 2.1. Flatter leg angles tend to be more robust to step-down disturbance. Steeper leg angles allow running at lower speeds and relate to handling larger push disturbances.

4.5.4. Swing-Leg Retraction

For fast running, the eigenvalue magnitudes are lower for slower retraction rates, illustrated in Figure 4.22. However, there are no stable limit cycles without swing-leg retraction. Fast-running limit cycles with low swing-leg retraction values have very minimal foot clearance. The robustness to step-down disturbance, illustrated in Figure 4.23 (top), increases with some swing-leg retraction. Step-down robustness is reduced for high retraction rates as the model starts missing the stance phase for large drops.

Robustness to push disturbance, shown in Figure 4.23 (middle), does not show a trend with varying leg retraction rate.

The ability to handle a pitch-rate disturbance improves when adding swing-leg retraction to the TSLIP model as shown in Figure 4.23 (bottom).

4.6. Control Strategy Comparison

The passive TSLIP model has stable gaits for a range of mass offsets where $r > 0$, as shown in Figure 4.24. Global PD control on pitch angle demonstrates neutrally stable limit cycles. The pitch and pitch-rate modes are stable. The system is neutrally stable when perturbed in the horizontal velocity.

The local velocity control shows asymptotically stable behaviour. There is a wide range of

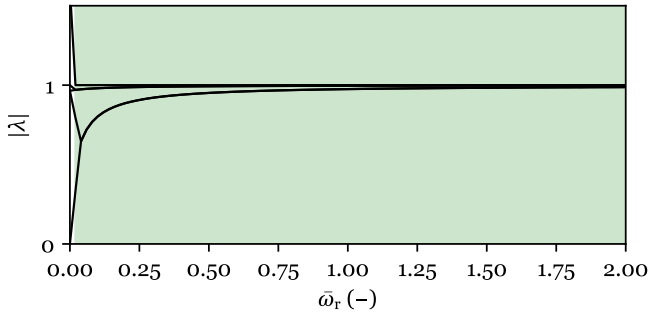

Figure 4.22: Eigenvalue magnitudes for the TSLIP model over varying normalized swing-leg retraction rates. Stable domain is marked in green. Configuration as in Table 2.1. Some swing-leg retraction is required for stability, but high retraction rates have a destabilizing effect.

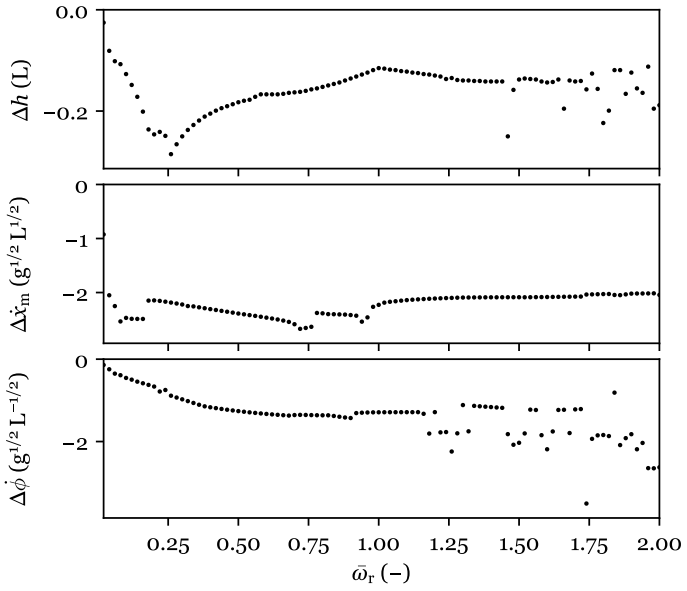

Figure 4.23: TSLIP robustness to step-down (top), horizontal push (middle), and pitch-rate disturbance (bottom) for the four different control strategies over varying normalized swing-leg retraction rates. Configuration as in Table 2.1. Adding swing-leg retraction improves step-down robustness, but high retraction rates are associated with falls due to missing the stance phase. The robustness to pitch-rate disturbance also improves with swing-leg retraction.

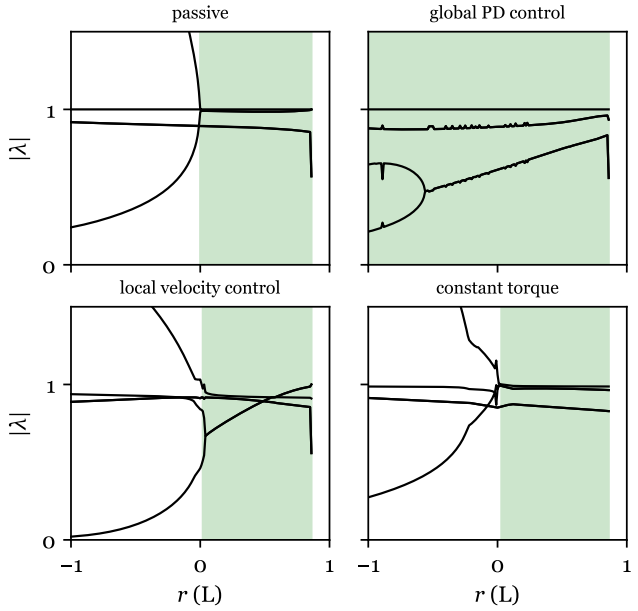

Figure 4.24: Eigenvalue magnitudes of the TSLIP model over changing mass offset for the four different control paradigms. Green areas mark the stable domain. Model configuration in Table 2.1. Self-stable gaits without inertial reference exist for mass offsets below the hip.

mass offsets for which there are stable limit cycles. Most of these are for $r > 0$. There exist a mass offset that is optimal for stability.

With a constant driving torque and leg damping the gait is neutrally stable to pitch angle disturbances. There are stable limit cycles for the centre of mass above the hip ($r < 0$), however these are not robust to perturbations.

The robustness limits for the four control strategies with respect to varying mass offset are shown in Figure 4.25. Global PD control provides the best robustness performance in general. For most mass offsets below the hip, the controllers perform similarly in response to a step-down (Figure 4.25 (top)).

In response to velocity disturbance, the passive, global-PD-controlled, and constant-driving-torque model perform similarly as illustrated in Figure 4.25 (middle). The local velocity control is least robust to sudden changes in velocity.

The global PD controller is able to deal with a significantly larger pitch-rate disturbance than the other three control methods, which have similar maximum pitch-rate disturbances as show in Figure 4.25 (bottom).

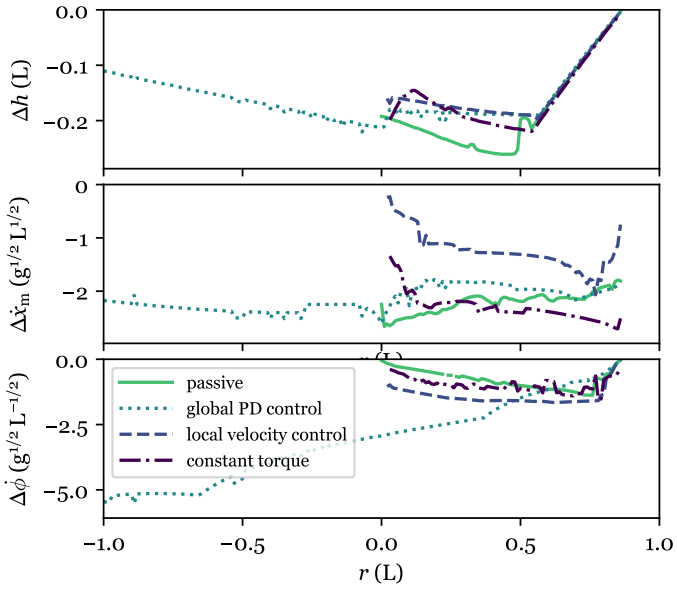

Figure 4.25: TSLIP robustness to step-down (top), horizontal push (middle), and pitch-rate disturbance (bottom) for the four different control strategies over varying mass offset. Model configuration in Table 2.1. Hanging mass configurations exhibit robust behaviour without explicit inertial references. The local velocity controller is less robust to a push disturbance.

5

Experimental Methods

5.1. HexRunner

The IHMC HexRunner shown in Figure 5.1 was designed with its body suspended from the central axis of rotation, which functions as a hip. The robot has six straight legs with telescoping springs, which are configured like a rimless wheel. There are three on each side that alternate contact as it runs.

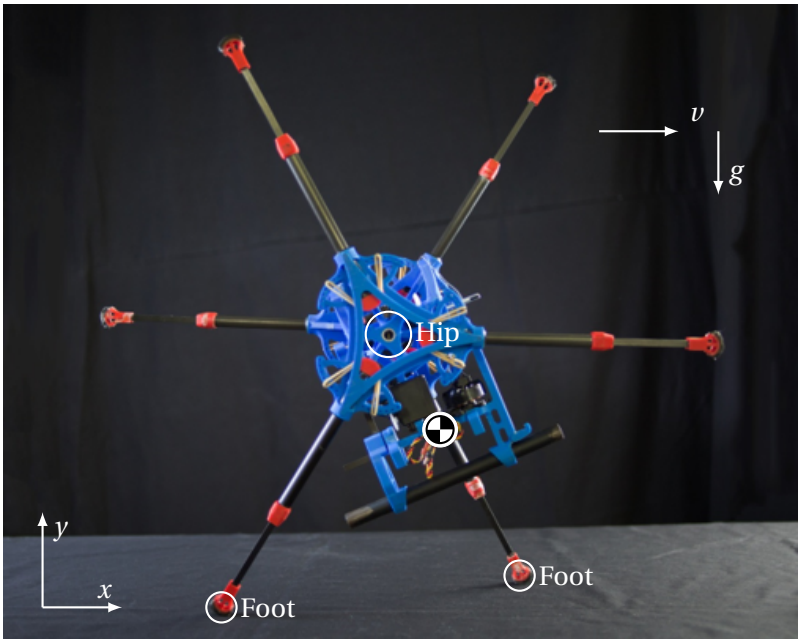

Figure 5.1: Image shows the HexRunner robot whilst it is standing still. It has six telescoping spring legs centrally driven from a single motor that is voltage-controlled by a human operator. It is launched using a pendulum swing to attain sufficient initial speed for running. The robot has no sensors, so the full gait is the result of its implicit dynamics and interaction with the environment.

The rimless wheel configuration is very similar to the TSLIP model with instant leg reset at lift-off and swing-leg retraction in the flight phase. It is mechanically simple because it does not need to solve the problem of leg reciprocation.

The HexRunner is able to run unsupported if launched with sufficient initial velocity and can be steered by controlling the sideways angle of the hanging mass. The sagittal-plane stability may be explained using the TSLIP model. It derives at least part of its stability in the transverse plane from gyroscopic effects. The small HexRunner shown in Figure 5.1 runs approximately $5\,\mathrm{m\,s^{-1}}$ in open space and is robust to running in high grass and over small hills. A larger version of the HexRunner runs in free space on level ground at over $13\,\mathrm{m\,s^{-1}}$ and has hit speeds over $22\,\mathrm{m\,s^{-1}}$ on a treadmill.

5.2. Planar Elliptical Runner

The IHMC Planar Elliptical Runner is a planar bipedal running robot with reciprocating legs, shown in Figure 5.2, that demonstrates running on a planarized treadmill at a maximum velocity of $4.4\,\mathrm{m\,s^{-1}}$, corresponding to a fast-running index of 1.73. The approximate physical parameters are listed in Table 5.1.

Table 5.1: Approximate Planar Elliptical Runner parameters.

Parameter		Value	Unit	Value	Unit
Velocity	v_0	4.4	$\mathrm{m\,s^{-1}}$	2.0	$\mathrm{g^{1/2}\,L^{1/2}}$
Total mass	m	3.3	kg	1.0	M
Mass offset	r	0.15	m	0.3	L
Gravity	g	9.81	$\mathrm{m\,s^2}$	1.0	g
Leg length	l_0	0.5	m	1.0	L

The robot is designed to run with only implicit feedback from its mechanical design. There are no sensors to provide feedback or measurements. The single operator input is the remote control on motor voltage set by a human operator. The operator thereby controls output power and subsequently steady-state running velocity.

The hip joint is the highest point on the body, which means the centre of mass is suspended below the hip. The legs are compliant due to their light construction and feature a linear spring at the ankle joint. The linear leg spring is directed approximately towards the hip joint during the stance phase. The foot trajectory is determined by the leg kinematics, which is similar to the mechanism found in an elliptical exercise machine. The leg structure supports the weight of the robot in stance without requiring actuation.

The mechanical design of the Planar Elliptical Runner is illustrated in Figure 5.3. The elastic buffer element in the motor decouples the two legs which enables the single motor to drive both the left and right leg. The leg trajectory throughout the gait follows from the mechanical design of the linkages. The driving mechanism generates the reciprocating motion in the leg. The ankle spring provides the compliance during the stance phase support. It can be tuned with the number of rubber bands and the tension with which they are mounted.

5.3. Choice of Robot

The lack of sensors on either robot makes analysis more involved than the simulation. The Planar Elliptical Runner is used for gathering experimental data because the planarized treadmill offers a controlled measurement environment. Furthermore, its reciprocating leg function is more representative of general bipedal running than the rimless wheel configuration.

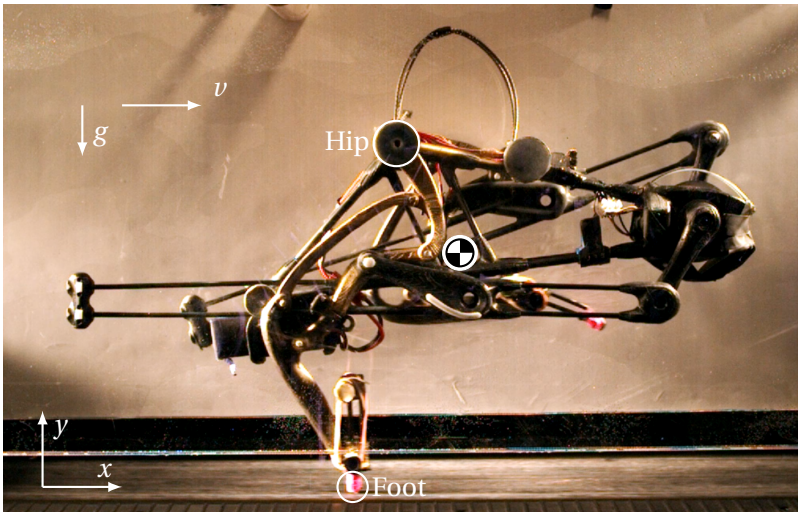

Figure 5.2: Still image showing the middle of the stance phase, taken from the high-speed video of the Planar Elliptical Runner running up to 4.4 $\mathrm{m\,s^{-1}}$ on a treadmill, planarized with two clear acrylic sheets. The image is mirrored horizontally to correspond with the other illustrations in this paper. The robot is centrally driven from a single motor that is voltage-controlled by a human operator to match the treadmill speed. The robot has no sensors, so the full gait is the result of its implicit dynamics and interaction with the environment.

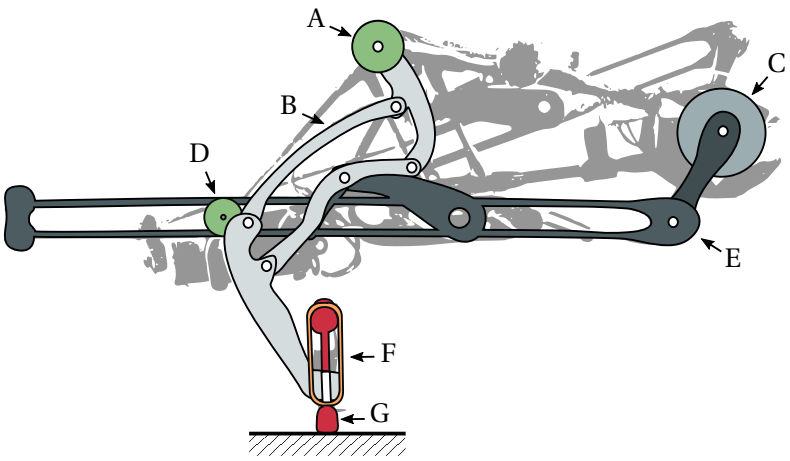

Figure 5.3: Illustration of the mechanical design for the Planar Elliptical Runner. The elements in the image are: A. hip joint, B. leg mechanism, C. driving motor with an elastic buffer element, D. fixed guide wheel, E. driving mechanism, F. rubber ankle spring, G. foot.

5.4. Experiment Set-up

The elliptical runner is set up on a treadmill running at a nominal velocity of $4.4\,\mathrm{m\,s^{-1}}$. The treadmill is planarized by setting up two clear acrylic sheets along the sides. The robot is supported against the acrylic sheets by circular, Teflon-covered supports that are fitted to the robot body. This prevents falling in the frontal plane, but some roll and yaw is still possible due to small gaps between the sheets and the supports, as well as compliance in the system.

The human operator drives the robot to stay in approximately the same position on the treadmill, so that it stays in the field of view of the camera. The camera takes video at a frame-rate of 1000 Hz. The recorded frame size is 1024 px wide by 816 px high, corresponding to 0.88 m wide by 0.70 m high at the side of the robot closest to the camera.

5.5. Motion Tracking

High-speed video imaging combined with digital image-processing techniques allows tracking of points on the body. Acquisition of position data is done with the OpenCV 4.0 computer-vision toolbox in Java.

The discs used to stabilize the body in the transverse direction are used as markers for the body position and orientation. A Canny edge-detection algorithm is applied on the frame converted to grey-scale. A Hough transform is then used to locate the circular markers on the processed frame. The transform is tuned to the size of the markers. The frame is cropped to a region of interest to prevent false positives.

A background subtraction algorithm is used to mask most of the stationary elements in the image as a basis for tracking the foot points. The feet have been marked with a specific colour. A mask based on an HSV colour range tuned to the foot colour is applied to the frame with the background subtracted. Ellipses are then fit around the bobs in the masked frame. The two largest ellipses are selected to be the foot positions.

For data series continuity, the body and foot points are appended to the series based on Euclidean distance to the last known points.

5.6. Position-Data Processing

The position data as it comes from the digital image processing contains noise and outliers due to imperfections in the point tracking. There are also gaps in the hind-foot position as it is occluded by the robot body.

The position data is checked for outliers by comparing the dataset to the same dataset with a low-pass filter applied. The points that are beyond a threshold value from the low-pass filtered data are discarded from the original dataset.

The centre-of-mass position, pitch angle, leg length and leg angle are computed from the position datasets.

The position data is not smooth enough to directly compute the velocities. A Savitzky-Golay filter is applied so that the gradients can be computed (Savitzky and Golay, 1964).

The stance phase and flight phase are determined by comparing the foot points to a ground reference representing the treadmill surface. The data is then separated into chunks per step, from touch-down to the next touch-down. The steps for which the foot closest to the camera is on the ground are then averaged and the standard deviation is taken. The steps where the hind

foot is in stance are discarded because of body roll and yaw and lack of data due to the body occluding the hind leg.

5.7. Model Fitting

The step-averaged results from the Elliptical Runner video are compared to a TSLIP simulation. A TSLIP model with a local angular velocity controller and leg damping is tuned manually to match the experimental results.

Local angular velocity control on the hip angle provides a simple model for the physical behaviour of a voltage-controlled electric motor that drives the hip. The motor throttle behaves similar to angular velocity control. Damping in the leg models the energetic losses due to impact, friction, and other inefficiencies in the running robot. The leg behaviour in flight phase is also locally defined, similar to how the robot leg kinematics are driven without inertial references.

The quality of the model fit is quantified using the Pearson correlation coefficient ρ,

$$\rho = \frac{\mathrm{cov}(y, \hat{y})}{\sigma_y \sigma_{\hat{y}}}, \tag{5.1}$$

for the measured signal y and the model estimate $\hat{y}$, with the covariance, cov, and the signal standard deviation, σ.

We also calculate the Variance Accounted For (VAF),

$$\mathrm{VAF} = \left(1 - \frac{\mathrm{var}(y - \hat{y})}{\mathrm{var}(y)}\right) \cdot 100\%, \tag{5.2}$$

with the signal variance, var.

Due to a limited availability of running data, fitting the model and quantifying the quality of the model fit is performed on the same data.

5.8. Modelled Response to Pitch Disturbance

A metacentric model for pitch stabilization is expected to be applicable to the Planar Elliptical Runner to explain its open-loop stability.

We take the TSLIP model fit to the measurements of the running robot, then subject the model to both a positive and a negative change in body pitch angle, after which we plot the ground reaction forces and resultant impulse. This response is compared to the metacentric models.

Due to a limited availability of running data, fitting the model and quantifying the quality of the model fit is performed on the same data.

6

Experimental Results

6.1. Measurements and Model Fit

The Planar Elliptical Runner runs at speeds of $1.2\,g^{1/2}\,L^{1/2}$ to $2.0\,g^{1/2}\,L^{1/2}$ without falling. At top speed it runs with a consistent aerial phase and may be considered fast running with a fast-running index of 1.73. At low speeds, it may run with alternating grounded and aerial running steps because of asymmetry.

The trial with the Planar Elliptical Runner has a total of 38 recorded steps. The recording was started after the robot held a steady position in view of the camera on the moving treadmill set to $4.4\,m\,s^{-1}$. The analysis only uses the 19 full steps where the leg closest to the camera goes through a stance phase.

Figure 6.1 shows a comparison between the average measurements of the Planar Elliptical Runner and a tuned TSLIP model. The model parameters are listed in Table 6.1. The model has been fit such that the stance duration t_s and the flight duration t_f correspond with measured data to within $0.01\,g^{-1/2}\,L^{1/2}$. The relevant stride parameters are listed in Table 6.2. Correlation and VAF are used to quantify the model fit as listed in Table 6.3, with the same data that was used to tune the model.

Table 6.1: TSLIP model fit to Planar Elliptical Runner. The model has leg damping and uses a local angular velocity controller on the hip angle.

Parameter		Value	Unit
Initial velocity	v_0	1.90	$g^{1/2}\,L^{1/2}$
Inertia	J	0.10	$M\,L^2$
Mass	m	1.00	M
Mass offset	r	0.30	L
Leg stiffness	k	8.00	$M\,g\,L^{-1}$
Touch-down angle	β_0	0.93	rad
Swing-leg retraction rate	ω_r	1.50	$rad\,g^{1/2}\,L^{-1/2}$
Damping coefficient	c	0.32	$M\,g^{1/2}\,L^{-1/2}$
Derivative gain	K_d	0.40	$M\,g^{1/2}\,L^{3/2}\,rad^{-1}$
Controller reference	$\dot{\alpha}_r$	2.42	$rad\,g^{1/2}\,L^{-1/2}$

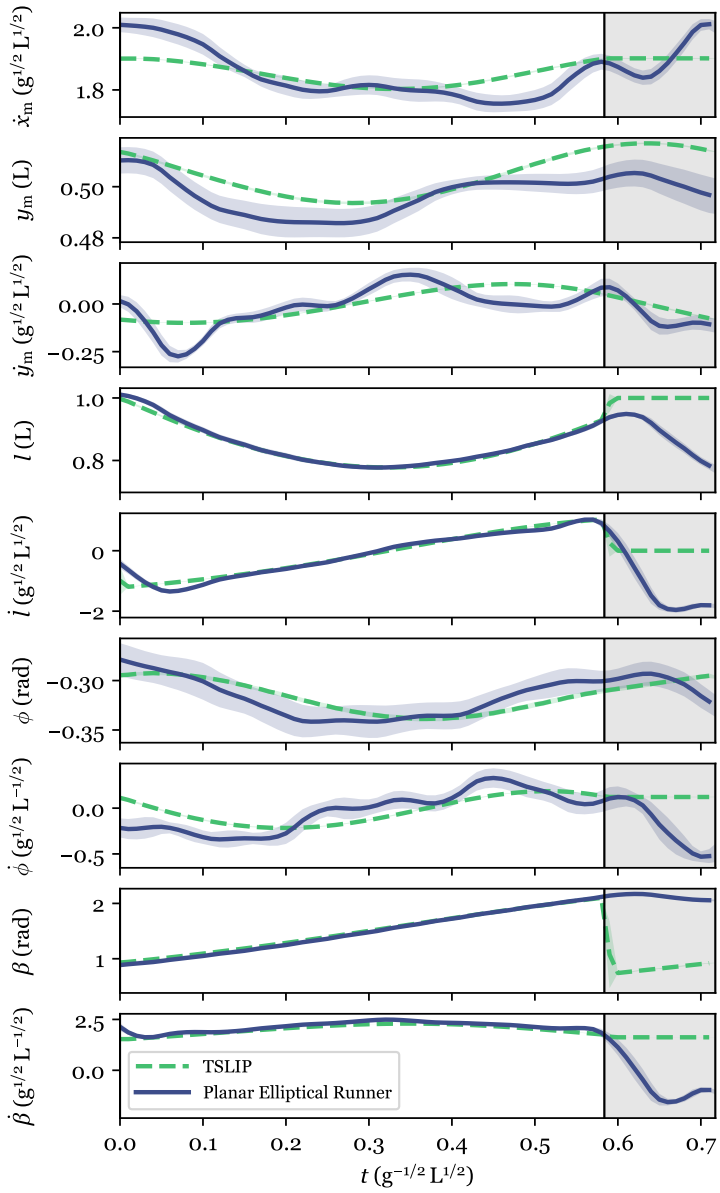

Figure 6.1: Step-averaged elliptical runner measurements compared to the TSLIP model. The model is manually tuned to match the stride times and state trajectories, yielding the configuration in Table 6.1, with the stride times listed in Table 6.2. The model fit is quantified in Table 6.3. The graph shows the mean behaviour averaged over 19 steps with the associated standard deviation. A step starts at touch-down and ends at the next touch-down. The flight phase is marked in grey. The model matches quite well in the stance phase, but there are some essential differences in flight-phase behaviour. The globally referenced states show significantly more variance than the TSLIP model.

Table 6.2: Mean stride times for Planar Elliptical Runner and TSLIP model fit. The model has been tuned to match the experimental times to within $0.01\,g^{-1/2}\,L^{1/2}$.

Parameter		Ell. Runner	TSLIP	Unit
Stance duration	t_s	0.58 ± 0.03	0.58	$g^{-1/2}\,L^{1/2}$
Flight duration	t_f	0.13 ± 0.02	0.13	$g^{-1/2}\,L^{1/2}$
Duty factor	d	0.81 ± 0.02	0.82	–
Step frequency	f	1.40 ± 0.07	1.41	$g^{1/2}\,L^{-1/2}$

Table 6.3: Quantification of the model fit using correlation (Corr) and Variance Accounted For (VAF), comparing the step-averaged results from the Planar Elliptical Runner with the tuned TSLIP model. The measures are computed separately using only stance-phase data and for the full stride including the flight phase.

		Stance		Full stride	
Parameter		Corr.	VAF	Corr.	VAF
Vertical pos.	y_m	0.847	71.6 %	0.808	53.5 %
Leg length	l	0.995	98.7 %	0.720	38.7 %
Leg angle	β	1.000	99.8 %	0.254	−46.4 %
Pitch angle	ϕ	0.790	62.2 %	0.766	61.0 %
Horizontal vel.	$\dot{x}_m$	0.771	46.4 %	0.744	45.6 %
Vertical vel.	$\dot{y}_m$	0.675	44.9 %	0.696	49.1 %
Leg length vel.	$\dot{l}$	0.977	95.6 %	0.696	53.9 %
Leg angle vel.	$\dot{\beta}$	0.931	87.5 %	0.680	51.2 %
Pitch angle vel.	$\dot{\phi}$	0.687	46.0 %	0.400	8.7 %

For fitting the TSLIP model, the combination of leg angle, leg stiffness, and velocity were dominant to the stance-phase behaviour. Without damping, the average pitch angle was approximately zero. Including damping leads to a higher average pitch angle, which allows matching the average experimental pitch. The controller reference is the result of the numerical optimization for a fixed point; it controls the limit cycle at the specified velocity and accounts for losses due to damping.

The largest eigenvalue magnitude of the TSLIP model is 0.92 , indicating an asymptotically stable limit cycle. The maximum step-down is –0.12 L, maximum push disturbance is $-0.73\,g^{1/2}\,L^{1/2}$, and the maximum pitch-rate disturbance is $-1.50\,\text{rad}\,g^{1/2}\,L^{-1/2}$.

The TSLIP model is started on its stable periodic orbit and runs every step on that orbit. There are no external perturbations, so the standard deviation from the mean is zero.

The velocities computed from the Planar Elliptical Runner data show more fluctuation than the model, which is visible in Figure 6.1 and represented in the correlation values in Table 6.3. The horizontal velocity of the centre of mass, $\dot{x}_m$, shows a large difference with the modelled velocity in the stance phase. The other parameters are more accurately represented by the model response.

The leg length and leg angle deviate from the TSLIP trajectory in flight phase, but match closely in the stance phase. This is also evident in the difference between considering only the stance phase and the full stride for computation of correlation and VAF . The Planar Elliptical Runner has two legs which alternate the stance and swing phase. The TSLIP model on the other hand, has only a single leg which is instantly reset to the forward position upon lift-off.

6.2. Modelled Response to Pitch Disturbance

Subjecting the TSLIP model fit to the Planar Elliptical Runner to the same pitch disturbance as in Section 4.1 yields the ground reaction forces and ground reaction impulse as plotted in Figure 6.2.

The centre of mass shifts horizontally with respect to the hip due to the pitch disturbance. The point of application of the resultant ground impulse remains in approximately the same position with respect to the hip. Subsequently, the torque about the centre of mass from the resultant ground impulse is oriented to correct the pitch disturbance.

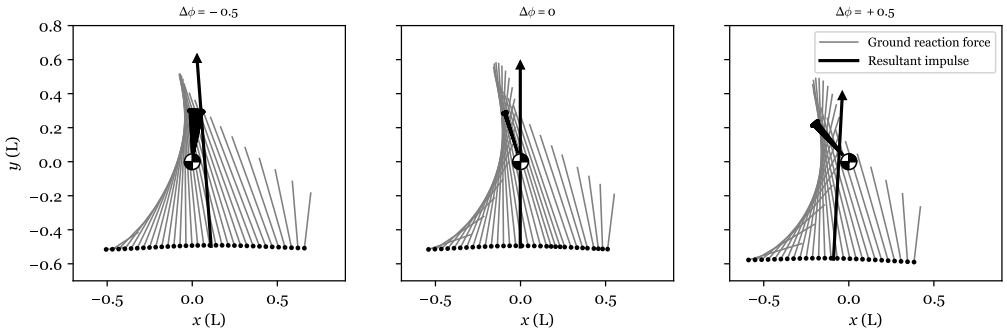

Figure 6.2: The TSLIP model fit to the measurements of the Planar Elliptical Runner is subjected to a disturbance in body pitch angle from the stable periodic limit cycle. All coordinates are taken with respect to the centre of mass. The model configuration is listed in Table 6.1. The direction of the ground reaction forces is shown as well as the resultant ground impulse. The impulse remains directed approximately towards the hip, which results in a torque about the centre of mass opposite to the pitch disturbance.

7

Discussion

7.1. Pendulum Configuration for Stable Pitch

7.1.1. Stabilizing Pitch

A necessary condition for pitch stability is that a pitch disturbance eventually results in a restoring torque about the centre of mass. The resultant impulse from the ground reaction forces in the TSLIP model is directed through the centre of mass in the unperturbed gait. The ground impulse can change either in direction or position to provide a restoring torque.

Running is a discrete system, so overcorrection is possible if the response to a pitch disturbance is too large. This is an important distinction because the metacentric stability concepts explain pitch stability either as a virtual pendulum or a floating vessel model. These are continuous systems which means that a larger restoring torque will result in faster convergence as eigenvalues approach negative infinity, instead of overcorrection as the discrete eigenvalue magnitudes exceed 1 for the running robot.

7.1.2. Metacentric Stabilization in TSLIP Running

The TSLIP model with a hanging mass and uncontrolled body pitch exhibits self-stabilizing gaits that are robust to disturbances. The resultant impulse from the ground reaction forces stays directed approximately towards the hip as a pitch disturbance is applied (Figure 4.2). The torque about the centre of mass then counteracts the disturbance in pitch. Overcorrection is avoided because the resultant ground impulse remains between the hip and centre of mass, thereby limiting the amount of torque and subsequent change in pitch rate that is generated.

The resultant ground impulse remains directed approximately towards the hip due to the model configuration. Ground reaction forces, as calculated in Equations (2.5) and (2.6), are applied at the foot and act through the leg, which is directed towards the hip. The direction of the ground reaction forces will not shift by much, unless a large torque is applied. The body pitch angle does not contribute to shifting the position of the ground reaction impulse unless a controller specifies a hip torque relative to the pitch angle. The suspension from the hip thus generates a stabilizing torque, that results in behaviour like the virtual pendulum, as illustrated in Figure 1.1 (d).

As the mass offset becomes too large, all gaits become unstable (Figure 4.24). This is proba-

bly because of the discrete nature of the running system. The impulse remains directed approximately towards the hip, but the large mass offset makes for a large moment arm when pitch is perturbed, thereby causing an excessive restoring torque which leads to overcorrection.

The global PD-controller can stabilize the body with a centre of mass above the hip by utilizing inertial measurements. The behaviour of the ground reaction forces in response to a pitch disturbance (Figure 4.3) is different than for the other control strategies. The direction of the impulse changes a lot in response to a pitch change because of the torque applied at the hip that actively stabilizes the body pitch. The resulting torque about the centre of mass does correct for the pitch disturbance without overcorrecting. The PD-controlled pitch response suggests that the metacentric stability concept does not necessarily represent pitch stability well if pitch is actively controlled with inertial measurements.

7.1.3. Mechanical Design for Pitch Stability

The TSLIP model tuned to the Planar Elliptical Runner displays a response to pitch disturbance that generates a stabilizing torque from the ground reaction forces. The robot has a configuration similar to the model with its centre of mass supported below a physical hip point. The ground reaction forces are directed through the legs similar to how the TSLIP model functions. This indicates the metacentric model may explain how the Planar Elliptical Runner maintains body pitch stability.

Maus et al. (2008) and Sharbafi et al. (2013) describe a Virtual Pivot Point Controller (VPPC) to actively control the direction of the ground reaction forces. The virtual metacentre constructed in that manner also demonstrates the metacentric concept of pitch stability. If we consider the combination of TSLIP model results, experimental results from the Planar Elliptical Runner, and the VPPC pitch control, self-stable body pitch may also be achieved through a mechanical robot design which constructs a virtual hip point by directing the leg force towards a metacentre throughout the stance phase.

7.2. Height and Velocity Stabilization

The passive TSLIP model is conservative, so any change in potential energy results in a change in kinetic energy and vice-versa. The main contributor to the kinetic energy in the model is its forward velocity; its vertical velocity averages zero for periodic running and so does the body pitch angular velocity. Potential energy is fully determined by the centre-of-mass height as long as the leg spring remains uncompressed.

Following a step change in ground height, we observe an opposite phase oscillation between centre-of-mass height and velocity (Figure 4.5). This is the result of an exchange between kinetic and potential energy due to the conservative nature of the model. Height and velocity show convergence over this multi-step oscillation, thereby illustrating stabilization.

A step-down change in ground height causes a faster downward velocity at touch-down, which then results in a ground impulse that is directed more forward (Figure 4.7). This causes an increase in the centre-of-mass velocity, thereby transferring energy from vertical, downward motion to horizontal, forward velocity. The lift-off trajectory is more horizontal as a result, which leads to an opposite effect on the next step, where some forward motion is exchanged for vertical, upward velocity. This behaviour is illustrated over multiple steps in Figure 4.6, and matches the SLIP model with swing-leg retraction (Seyfarth, 2003). Applying a swing-leg retrac-

tion rate in the flight phase can enhance this exchange of energy and improve convergence, if a suitable, neither too low, nor too high, retraction rate is chosen.

This energy-exchange mechanism results in a stabilizing oscillation, where the average height above ground converges as determined by the definition of the model kinematics without requiring damping in the leg or explicitly controlling for centre-of-mass height. The stabilizing behaviour of the centre-of-mass height implies velocity is stable as well, with any change in potential energy leading to a subsequent change in forward velocity.

7.3. Fast Running

A trade-off to the reduced stability and step-down robustness for fast running is the increased parameter space of possible leg stiffness and touch-down angles for self-stable gaits (Figure 4.10). This matches the behaviour of the spring-mass model without a trunk (Seyfarth et al., 2002; Geyer et al., 2006). The wide range of possible leg touch-down angles indicates that foot placement becomes non-critical for fast running. This allows the same kinematic configuration to be used at different speeds, as is also evident from the large velocity domain that has stable limit cycles for a fixed TSLIP configuration (Figure 4.8).

The primary change required for changing the running velocity is the reference angular velocity or the driving torque at the hip.

7.4. Damping in the Leg or Hip

Introducing damping in the leg (Figure 4.12) or at the hip (Figure 4.14) improves stability of the running system. The constant torque compensates for the energy dissipated so that the gait converges to a periodic limit cycle. Both leg and hip damping are associated with decreasing eigenvalues, but they do not not necessarily affect the dominant unstable mode. Leg damping primarily influences stabilization of the centre-of-mass height, and thereby also velocity. Damping at the hip is beneficial to pitch stability. Both leg and hip damping should therefore be combined for robust self-stable running.

Hip damping improves robustness to a pitch-rate disturbance, but apart from that neither leg nor hip damping are beneficial to robustness. The parameters that yield the best limit-cycle stability for the running gait do not need to be the parameters that make the system most resistant to falling; maximum stability and maximum robustness require a different parameter choice.

7.5. Effects of Parameter Choice

7.5.1. Mass Offset

Having the mass offset below the hip is required for stability and robustness with locally defined control because of the pendulum-like stabilization of body pitch. The mass offset has minimal influence on the stability of the passive model, but there is an optimal mass offset for stability with the local velocity controller. When prioritizing robustness, a mass offset between 0.2 L and 0.5 L yields the best results for robustness over the different control strategies. The TSLIP model becomes unstable as the mass offset exceeds 0.86 L, which is likely due to overcorrection in the discrete running system.

7.5.2. Stiffness and Leg Angle

The maximum push disturbance increases with decreasing stiffness (Figure 4.19) and with steeper leg angles (Figure 4.21). The leg stiffness and touch-down angle are the main factors for determining the minimum velocity for stable running gaits. This makes the leg configuration an important factor for design for running at a desired speed.

The choice of stiffness and leg angle is not critical for stability (Figure 4.18, 4.20), but does have an effect on step-down robustness. At a given velocity, stiffness and leg angle can be chosen in a combination to maximize step-down robustness.

Adjustable leg stiffness could provide the required change to maintain robust running for varying velocities. A time-based leg-stiffening strategy could improve the step-down robustness (Palmer et al., 2014). This could be achieved by adjustable springs or antagonistic actuation (Hosoda et al., 2008). A non-linear leg stiffness may also be tuned to provide a large improvement in robustness to ground-height variation (Karssen and Wisse, 2011). Control of leg stiffness can also be use to control forward velocity during running (Bertrand, 2012).

7.5.3. Swing-Leg Retraction

Angular retraction of the leg during flight phase contributes to stability and robustness of the TSLIP model (Figures 4.22, 4.23). The retraction rate makes the touch-down angle dependent on flight duration and thereby improves stability. Shorter flight durations result in flatter touch-down angles of the leg, leading to a more vertical lift-off and a longer flight phase on the next step. The opposite happens for a longer flight duration, leading to a stabilizing oscillating behaviour from swing-leg retraction. Implementing swing-leg retraction stabilizes gaits that would be unstable for fixed leg angles, similar to the effect on the SLIP model (Seyfarth, 2003). The optimal swing-leg retraction rate differs with leg type (Karssen et al., 2015) and will thus need to be tuned to the specific application instead of directly applying the TSLIP model results to robot design.

Another reason for improvement in robustness is that swing-leg retraction improves ground clearance, which would otherwise be minimal and cause tripping even for small disturbances. This corresponds with the behaviour for the SLIP model with swing-leg retraction (Ernst et al., 2012). Ground clearance is less of a problem for a two-legged model because the swing-leg will need to be shortened anyway for the forward swing-through. Such a model will still have the advantage to stability from applying a swing-leg retraction rate.

A downside to applying a constant retraction rate is that it becomes possible to miss the stance phase for large step-down changes in ground height. This is also represented in the normalized maximum drop defined by Daley and Usherwood (2010) which depends on retraction rate and leg stiffness. Stopping swing-leg retraction at a certain angle could be a strategy for avoided missing a step.

7.6. Control Without Inertial Reference

Most spring-mass running models are based on the SLIP model (Blickhan, 1989) which uses an inertial reference angle for its leg reset upon lift-off. Robots commonly have inertial measurement units (IMU) to measure their orientation in the world and depend on feedback control to stabilize the trunk orientation.

The TSLIP model has self-stable running gaits without any explicit inertial measurements

with the centre of mass offset below the hip. This self-stable body configuration allows the leg angle reset upon lift-off and swing-leg retraction rates to be defined as local hip angles.

The stable running gaits for the hip-driven TSLIP model are in line with the findings by Shen et al. (2014) that demonstrate a positive stabilizing effect for rotary forcing in the SLIP model.

The angular velocity of the stance leg is determined by the horizontal velocity during the stance phase. This can be combined with the consistent body orientation to relate the hip angular velocity to forward velocity. The local hip angular velocity controller thus becomes a velocity controller through implicit feedback from the system dynamics when pitch is stable. Neville et al. (2006) describes a similar concept but applies an inertial reference to control body pitch.

Applying velocity control through controlling the local hip angular velocity means that the TSLIP model is able to run without neutrally stable modes (Figure 4.24). The downside is that it is less robust to velocity disturbance (Figure 4.25) because a spike in control torque will lead to a fall if the difference between limit cycle velocity and actual velocity is too large.

The Planar Elliptical Runner demonstrates the practical application of the local control principles discussed here. The leg kinematics of the Planar Elliptical Runner are defined relative to its body by its mechanical design. This means that its steady body pitch angle provides a constant reference for the rest of its dynamic behaviour. This is similar to what is observed for the TSLIP model with hanging mass and local angle referencing. The physical behaviour of the voltage controlled electric motor is similar to the TSLIP control on the hip angular velocity. The motor throttle is analogous to setting the reference angular velocity in the model. This leads to the Planar Elliptical Runner having global velocity controlled via its intrinsic dynamics.

7.7. Modelling the Planar Elliptical Runner

The TSLIP model with local angular velocity control and leg damping can model the behaviour of the Planar Elliptical Runner at top speed, as illustrated with the comparison of the mean state behaviour per step in Figure 6.1.

The Planar Elliptical Runner does roll and yaw a little as it runs, which disturbs some of the state variables. This affects the mean measurements because completely planar motion is assumed and only one side of the robot is fully visible. For example, the mean end of stride height of the centre of mass does not match with the start of the stride.

The model response correlates well with the mean measured step behaviour in stance phase (Table 6.3). The correlation is better for locally measured states, i.e. leg length and leg angle, than for global states, i.e. centre-of-mass height, pitch, and velocity. The measurement of global states is subject to more disturbances, resulting in more variance than is present in the TSLIP model.

The correlation for the full stride is not as good because the TSLIP model has only one leg. The Planar Elliptical Runner needs to shorten its leg to be able to swing it forward, whereas the TSLIP model leg is reset instantly to its resting length and reference angle upon lift-off. This explains the large differences and poor correlation for leg angle and leg length between model and experimental results for the full stride.

The absence of a second leg means grounded running gaits are not possible in the TSLIP model. This has an effect on the lower velocity limits and robustness, as it is unable to take a

double-stance step or compensate a missed stance phase with its second leg. Having only one leg does not invalidate results for running with an aerial phase. However, the fact that the model only has a single leg means that it can not be used to model the dynamics of the swing leg. This problem is the same for the canonical SLIP model. It has been handled by either implementing a second leg to enable grounded running (Geyer et al., 2006) or by adding a small pendulum to represent the swing leg (Rashty et al., 2014).

Taking into account the limits of a one-legged model, the results for centre-of-mass trajectory, stance-phase behaviour, and stability and robustness can be applied to fast bipedal running.

7.8. Future Research

The theoretical foundations in sagittal-plane running should be used to drive design and develop experimental fast running robotics.

Additionally, extending the robustness and stability analysis to a two-legged model in the sagittal plane could provide further insight into fast-running behaviours because it introduces the capability for a double-stance phase, and thus grounded running, and the ability to miss a stance phase with a single leg without falling.

Other strategies such as non-linear stiffness, leg-length variation, and variable leg retraction speeds may be applied to improve running stability and robustness.

Starting from sagittal-plane stability, concepts for fast three-dimensional running should be developed. Implementing lateral stability, especially in the context of self-stability, is still an open problem. One possible direction is to design the running dynamics to introduce a roll-yaw coupling similar to the mechanism that allows bicycles to self-stabilize with sufficient forward velocity.

The mechanisms that enable the self-stable planar bipedal running in simulation and experimental robotics may also be present in biological running. Ostriches, for example, might generate a metacentric pivot point to self-stabilize their body pitch. This could be tested with measurements of ground reaction forces in running birds subjected to a disturbance in body pitch.

8

Conclusion

A metacentric model can be used to explain pitch stability in the TSLIP model and the Planar Elliptical Runner. The body mass acts as a consistent world reference when suspended below a hip pivot point. This enables stable running without inertial measurements, utilizing only local references. Subsequently, robots could do without an IMU for stable and robust running if their mechanical design facilitates implicit control.

No complex control algorithms are required to control running velocity. Centre-of-mass height and velocity are stable even without feedback or damping. Body-pitch stability and implicit feedback from leg dynamics allows speed control based on the angular velocity at the hip. Similarly, the TSLIP model with a constant driving hip torque coupled with a damping element in the hip or leg will stabilize to a predictable velocity.

Self-stable fast running is possible for a larger number of parameter configurations than slow running. Foot placement becomes less critical with greater speed, thus less precise control may suffice.

For practical running robotics, robustness is more important than stability, once stability has been achieved. Running with a specific limit cycle achieves little if a small disturbance results in a fall. However, limit-cycle stability does provide a good starting point for evaluating the feasibility of a running gait.

A

Derivation of the Equations of Motion

The derivation of the equations of motion for the stance phase is done using the TMT method (Vallery and Schwab, 2019) and verified with an independent derivation using Lagrangian dynamics.

The full system coordinate vector $\boldsymbol{x}$ is defined to be:

$$\boldsymbol{x} = \begin{bmatrix} x_\mathrm{m} & y_\mathrm{m} & l & \beta & \phi \end{bmatrix}^\mathrm{T}. \tag{A.1}$$

In stance phase, the foot is fixed and the entire system can be described with the minimal coordinate vector $\boldsymbol{q}$,

$$\boldsymbol{q} = \begin{bmatrix} l & \beta & \phi \end{bmatrix}^\mathrm{T}. \tag{A.2}$$

The kinematic transformation $\boldsymbol{T}(\boldsymbol{q}) : \mathbb{R}^3 \rightarrow \mathbb{R}^5$ describes the transformation from minimal coordinates to the full set of coordinates,

$$\boldsymbol{x} = \boldsymbol{T}(\boldsymbol{q}) = \begin{bmatrix} -l\cos(\beta) + r\sin(\phi) + x_\mathrm{f} \\ l\sin(\beta) - r\cos(\phi) + h \\ l \\ \beta \\ \phi \end{bmatrix}. \tag{A.3}$$

The Jacobian of the kinematic transformation $\mathbf{J}_\mathrm{T}$ is taken with respect to the minimal coordinates,

$$\mathbf{J}_\mathrm{T}(\boldsymbol{q}) = \frac{\partial \mathbf{T}(\boldsymbol{q})}{\partial \boldsymbol{q}} = \begin{bmatrix} -\cos(\beta) & l\sin(\beta) & r\cos(\phi) \\ \sin(\beta) & l\cos(\beta) & r\sin(\phi) \\ 1 & 0 & 0 \\ 0 & 1 & 0 \\ 0 & 0 & 1 \end{bmatrix}. \tag{A.4}$$

This Jacobian allows the computation of the full set of velocities $\dot{\boldsymbol{x}}$ from the minimal velocities $\dot{\boldsymbol{q}}$,

$$\dot{\boldsymbol{x}} = \mathbf{J}_\mathrm{T}(\boldsymbol{q})\,\dot{\boldsymbol{q}}. \tag{A.5}$$

The full mass matrix $\mathbf{M}_\mathrm{f}$ is a diagonal matrix with the body mass m and mass moment of inertia J,

$$\mathbf{M}_\mathrm{f} = \mathrm{diag}\left(\begin{bmatrix} m & m & 0 & 0 & J \end{bmatrix}\right). \tag{A.6}$$

This is reduced to the mass matrix in minimal coordinates $\mathbf{M}$ with the kinematic Jacobian,

$$\mathbf{M} = \mathbf{J}_\mathrm{T}^\mathrm{T}\mathbf{M}_\mathrm{f}\mathbf{J}_\mathrm{T} = \tag{A.7}$$
$$\begin{bmatrix} m & 0 & -mr\cos(\beta+\phi) \\ 0 & ml^2 & mrl\sin(\beta+\phi) \\ -mr\cos(\beta+\phi) & mrl\sin(\beta+\phi) & J+mr^2 \end{bmatrix}.$$

The force vectors are defined in the full set of coordinates. The gravitational acceleration g acts downward along the y axis. The applied force vector due to gravity $\boldsymbol{f}_\mathrm{g}$ is then

$$\boldsymbol{f}_\mathrm{g} = \begin{bmatrix} 0 & -mg & 0 & 0 & 0 \end{bmatrix}^\mathrm{T}. \tag{A.8}$$

The hip torque is defined in the positive direction for β and ϕ, yielding the hip torque vector $\boldsymbol{f}_\mathrm{t}$,

$$\boldsymbol{f}_\mathrm{t} = \begin{bmatrix} 0 & 0 & 0 & \tau & \tau \end{bmatrix}^\mathrm{T}. \tag{A.9}$$

The compressive leg force vector $\boldsymbol{f}_\mathrm{l}$ acts along the leg length,

$$\boldsymbol{f}_\mathrm{l} = \begin{bmatrix} 0 & 0 & F_\mathrm{l} & 0 & 0 \end{bmatrix}^\mathrm{T}, \tag{A.10}$$

where the force F_l follows from Equation 2.1. The sum of the force vectors is transformed to the force vector in minimal coordinates $\boldsymbol{Q}$ with the kinematic Jacobian,

$$\begin{aligned} \boldsymbol{Q} &= \mathbf{J}_\mathrm{T}^\mathrm{T}(\boldsymbol{f}_\mathrm{g} + \boldsymbol{f}_\mathrm{t} + \boldsymbol{f}_\mathrm{l}) \\ &= \begin{bmatrix} -mg\sin(\beta) + k(l_0 - l) - c_\mathrm{l}\dot{l} \\ \tau - mgl\cos(\beta) \\ \tau - mgr\sin(\phi) \end{bmatrix}. \end{aligned} \tag{A.11}$$

The convective accelerations $\boldsymbol{c}$ are computed,

$$\boldsymbol{c} = \left(\left(\frac{\partial \mathbf{J}_\mathrm{T}}{\partial \boldsymbol{q}}\right)\dot{\boldsymbol{q}}\right)\dot{\boldsymbol{q}}, \tag{A.12}$$

and transformed to the convective accelerations in minimal coordinates $\boldsymbol{C}$,

$$\begin{aligned} \boldsymbol{C} &= \mathbf{J}_\mathrm{T}^\mathrm{T}\mathbf{M}\boldsymbol{c} \\ &= \begin{bmatrix} mr\dot{\phi}^2\sin(\beta+\phi) - ml\dot{\beta}^2 \\ mrl\dot{\phi}^2\cos(\beta+\phi) + 2ml\dot{\beta}\dot{l} \\ mrl\dot{\beta}^2\cos(\beta+\phi) + 2mr\dot{\beta}\dot{l}\sin(\beta+\phi) \end{bmatrix}. \end{aligned} \tag{A.13}$$

The system of equations can be solved for the generalized accelerations $\ddot{\boldsymbol{q}}$ in stance,

$$\mathbf{M}\ddot{\boldsymbol{q}} = \boldsymbol{Q} - \boldsymbol{C}. \tag{A.14}$$

B

Eigenvalues of the Poincaré Map

Define P a function that takes the state $\boldsymbol{q}$ at the Poincaré section right after touch-down and returns the state at the next Poincaré section,

$$P(\boldsymbol{q}_n) = \boldsymbol{q}_{n+1}\,, \tag{B.1}$$

making it our stride-to-stride map.

To numerically evaluate stability, we evaluate the Jacobian of F with respect to $\boldsymbol{q}$ by means of a first order central difference method,

$$\boldsymbol{A}_i = \frac{P(\boldsymbol{q}^* + \Delta q_i) - P(\boldsymbol{q}^* - \Delta q_i)}{2\Delta q_i}\,, \tag{B.2}$$

where Δq_i is a perturbation on the i^{th} element of $\boldsymbol{q}^*$ and $\boldsymbol{A}_i$ is the i^{th} column of the map $\mathbf{A}$ that governs the dynamics of perturbations from limit cycles as

$$\Delta\boldsymbol{q}_{n+1} = \mathbf{A}\Delta\boldsymbol{q}_n\,, \qquad \text{with} \qquad \Delta\boldsymbol{q}_n = \boldsymbol{q}_n - \boldsymbol{q}^*\,. \tag{B.3}$$

The Floquet multipliers are the eigenvalues λ of the linearized, discrete, step-to-step map $\mathbf{A}$, such that,

$$|\mathbf{A} - \lambda\mathbf{I}| = \mathbf{0}\,. \tag{B.4}$$

C

Validity of the No-Slip Assumption

The TSLIP model simulations assume the foot does not slip during the stance phase. The validity of this assumption is checked by assuming a coefficient of static friction of $\mu = 1.0$ for dry rubber on concrete. The maximum force of friction F_f is then:

$$F_f = \mu F_y . \tag{C.1}$$

The maximum static friction is compared with the actual horizontal reaction force assuming the foot does not slip. Figure C.1 (left) shows that the magnitude of the horizontal ground reaction force is lower than the allowable friction for the passive TSLIP model. The ground reaction force for the TSLIP model fit to the Planar Elliptical Runner exceeds the allowable friction slightly at the end of the stance phase. Some slipping may occur in the last 10 % of the stance phase.

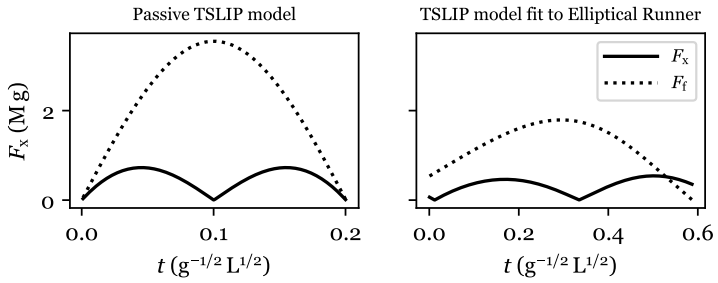

Figure C.1: Comparison between the actual ground reaction force and the maximum static friction force, assuming a coefficient of static friction of $\mu = 1.0$ for rubber on dry concrete. The passive TSLIP model (left), configuration in Table 2.1 does not exceed the allowable friction. The TSLIP model fit to the Planar Elliptical Runner (right), configuration in Table 5.1, slightly exceeds the allowable friction in the last 10 % of stance.

Contributions and Acknowledgments

Contributions

Maarten van den Broek developed and performed the analysis of the TSLIP model, recorded the measurements of the Planar Elliptical Runner, and combined the results into this paper. Jerry Pratt and Robert Griffin provided feedback throughout this study. Chris Schmidt-Wetekam worked on the design and fabrication of the Planar Elliptical Runner. Johnny Godowski provided the origin of the FastRunner concept, helped design and build the HexRunner, and contributed intuitive explanations of running stability with a hanging mass configuration, which Jerry Pratt helped translate into a mathematical formulation. Ken Chao performed a preliminary analysis on planar running stability.

Acknowledgments

Thanks to William Howell for recording the video of the Planar Elliptical Runner experiment and Sylvain Bertrand and Heike Vallery for their valuable feedback in the course of this study.

II

Appendices

Maarten J. van den Broek

Additional material that did not get included in the paper in Part I.

D

Supplementary Material

This chapter provides supplementary material for the paper included in Part I. Section D.1 expands upon the changes of stance behaviour with running velocity. An overview of the experimental design with the Planar Elliptical Runner is provided in Section D.2. The measured foot trajectory is provided in Section D.3. Illustrations for the motion-tracking algorithm are provided in Section D.4. Finally, some details on the processing of the raw position data are provided in Section D.5.

D.1. Effects of Speed on Stance Duration

For a spring-mass system with stiffness k and mass m that is hopping in place, the stance duration t_b is half of a full oscillatory period,

$$t_\mathrm{b} = \pi\sqrt{\frac{m}{k}}. \tag{D.1}$$

For a purely horizontal motion, stance duration is dominated by the leg angle, assuming a symmetric stance phase. The distance covered in stance is a result of touch-down angle β_0 and resting leg length l_0. Combining the distance with the centre-of-mass velocity yiels an estimate of the stance time t_s,

$$t_\mathrm{s} \approx \frac{2l_0(\pi/2-\beta_0)}{v_0}, \tag{D.2}$$

using a small-angle approximation to simplify the equation.

The centre-of-mass trajectory for the SLIP and TSLIP models becomes increasingly horizontal as running velocity increases. This becomes apparent in the difference in stance time as the speed increases. This change from a bouncy gait dominated by spring-mass behaviour to a more horizontal, velocity-dominated gait, may explain in part why the choice of leg stiffness and touch-down angle becomes less critical at high speeds.

D.2. Experimental Design

The measurements of the running behaviour of the Planar Elliptical Runner were obtained with the robot running on a regular treadmill. The complete set-up is illustrated in Figure D.1.

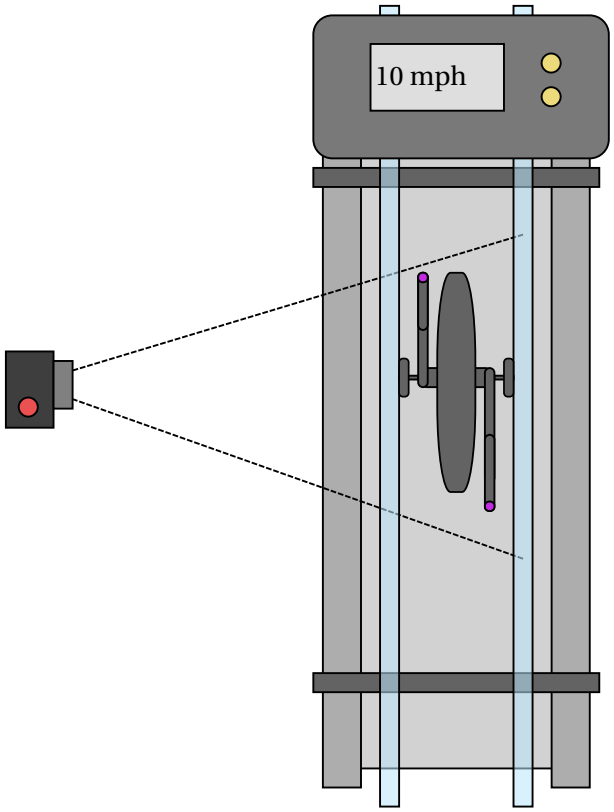

Figure D.1: Experimental set-up for measurements of the Planar Elliptical Runner on a treadmill. The camera is positioned to the left of the robot. The robot is laterally stabilized with Teflon-covered supports between two acrylic glass sheets. The sheets are held upright by two wooden supports. The operator controls the motor voltage to keep the robot within the field of view of the camera. The feet are marked with coloured tape for tracking.

The robot is kept upright with Teflon-covered supports between two acrylic sheets. These sheets are supported by two wooden supports on the treadmill. The right sheet is fitted with a large peace of white paper to provide an even background for the measurements. The camera is positioned on the left such that the robot fits within the field of view with some margin. The operator is able to reliably control the speed of the robot such that it remains within view of the camera for the duration of the recording.

Spotlights surround the experimental set-up to provide a well-lit environment. This allows high shutter-speeds to minimize motion blur in the recorded image.

The 1000 Hz frame-rate for the video recording is the maximum the camera was capable of. The resulting data contained more information for outlier rejection and estimation of state parameters than the 240 Hz or 500 Hz trials. High frequency position measurements were especially useful due to the smoothing required for velocity estimation.

D.3. Measured Foot Trajectory

The mechanism generates consistent foot trajectories as illustrated in Figure D.2, with the coordinates taken with respect to the centre of mass. There is a clear oscillation in the trajectory due to the leg compliance as the foot is swung forward.

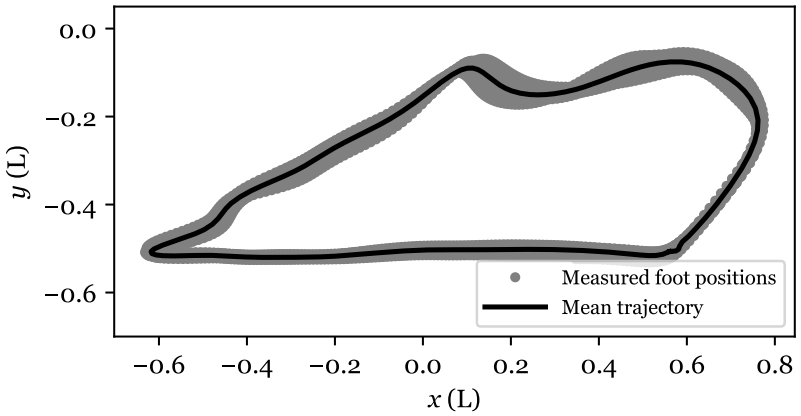

Figure D.2: Plot of the foot position measurements and mean trajectory of the Planar Elliptical Runner experiment. The coordinates are with respect to the centre of mass. The trajectory shows a consistent oscillation as the foot is swung forward.

D.4. Motion Tracking Details

This section provide some illustration for the motion tracking algorithm described in Section 5.5. Figure D.3 shows the steps taken for the tracking of the circular Teflon-covered supports that are used to support the Planar Elliptical Runner between the acrylic sheets. The steps for tracking the foot positions are illustrated in Figure D.4.

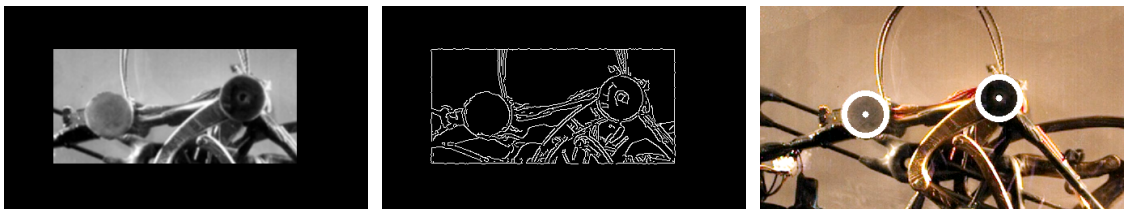

(a) **(b)** **(c)**

Figure D.3: Tracking of the circular Teflon-covered supports that define the body position and orientation of the Planar Elliptical Runner. **(a)** A region of interest is selected on the grey-scale version of the frame, based on the last known points. **(b)** A Canny edge-detection algorithm is applied to the masked region of interest. **(c)** Circles are then fit using a Hough transform to identify the position of the circular supports.

D.5. Processing of Position Data

The raw data from the motion-tracking algorithm contains outliers and noise. The outliers are removed by comparison to a low-pass-filtered copy of the dataset. Values beyond a threshold value from the smoothed data are rejected as illustrated in Figure D.5. High-frequency noise is then removed with a low-pass filter as illustrated in Figure D.6. The noise originates from slight fluctuations in the tracking algorithm and the discrete nature of the measurements, which rely on the image resolution.

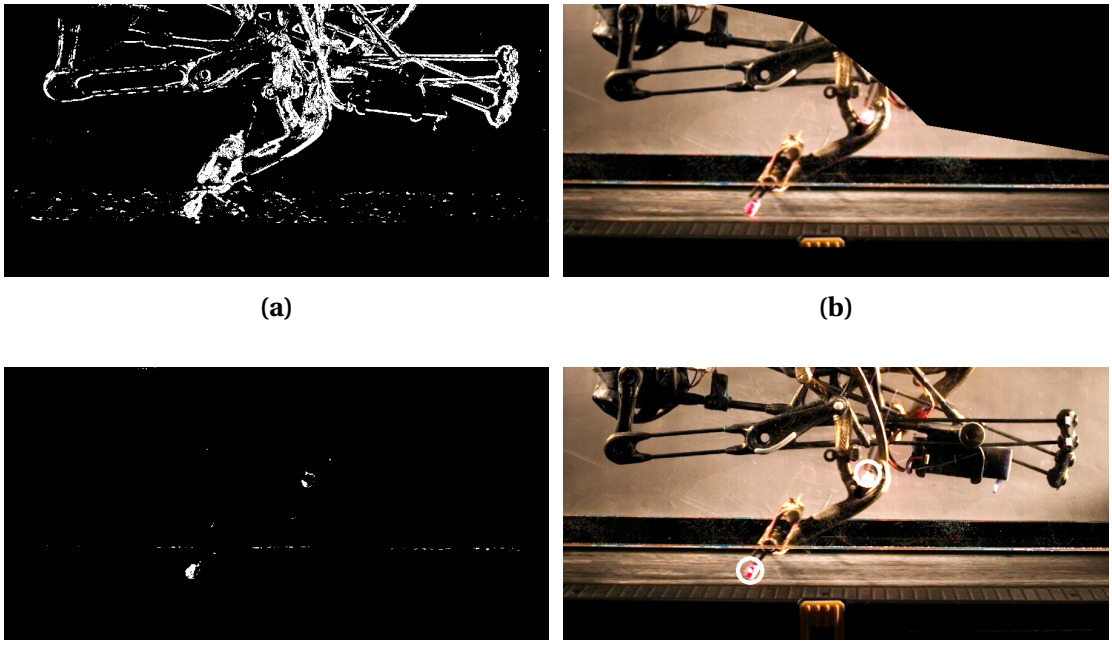

(a) **(b)**

(c) **(d)**

Figure D.4: Tracking of the colour-marked feet of the Planar Elliptical Runner. **(a)** The background-subtraction algorithm produces a mask that removes most of the static background elements from the frame. **(b)** A region of interest is selected from the full frame for tracking foot points. **(c)** After the background is masked from the region of interest, a HSV colour mask is applied that masks anything that is not the foot colour. **(d)** The two blobs with the largest area are then selected, where the centroid is recorded as the foot position.

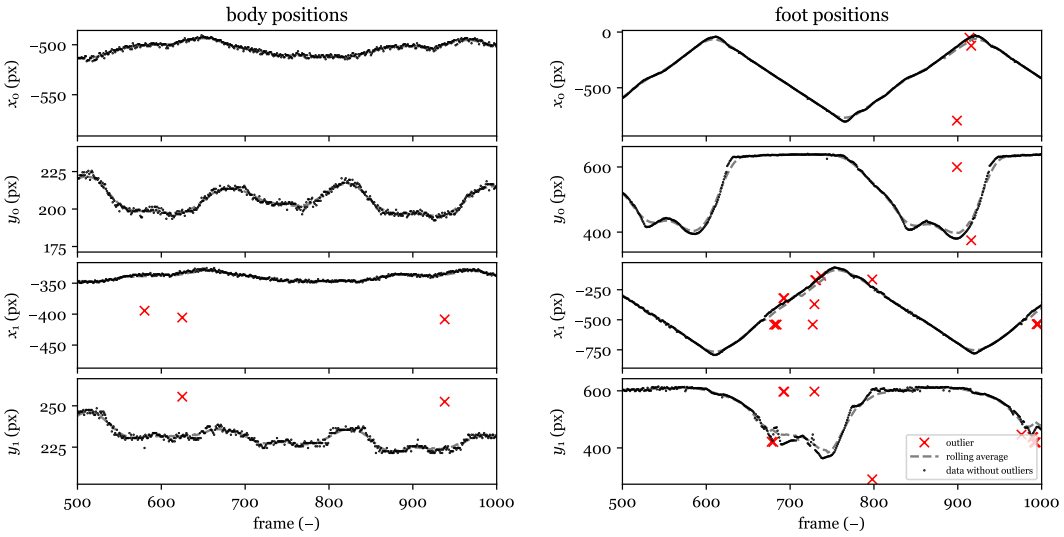

Figure D.5: Segment of the position data from the motion tracking of the Planar Elliptical Runner, illustrating the process of outlier rejection by comparison to a low-pass-filtered copy of the dataset.

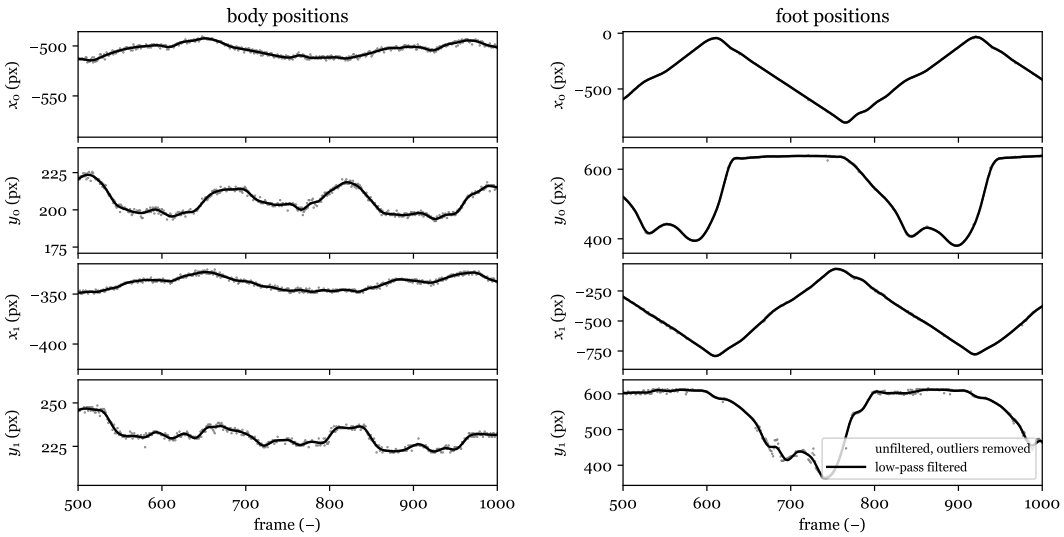

Figure D.6: Segment of the position data from the motion tracking of the Planar Elliptical Runner, illustrating the use of low-pass filtering to remove high-frequency noise.

E

Planar Running with Non-Massless Legs

E.1. Introduction

The spring-loaded inverted pendulum (SLIP) model has been used extensively to model running centre-of-mass dynamics. It may also be used as a foundation for extended running models. The SLIP model may be anchored in a model with leg masses and damping, whilst predominantly conserving the domain of leg parameters leading to self-stable running patterns (Peuker et al., 2012).

Passive body-pitch stabilization for bipedal running has been demonstrated with the TSLIP model and experimentally shown to be possible with the IHMC Planar Elliptical Runner. Using the TSLIP model as a starting point for design, we expect it to be possible to develop a planar bipedal running model with leg mass that demonstrates similar self-stability, especially with respect to trunk stabilization.

Section E.2 describes the design of a bipedal running model and a parametric controller for leg reciprocation. The methods for analysis of this model are described in Section E.3, followed by the results in Section E.4. The results are discussed in Section E.5, with the conclusions in Section E.6.

E.2. Two-Legged Running Model

E.2.1. Model Description

The two-legged running model is illustrated in Figure E.1. It consists of a body and two legs with each a thigh, shank, and foot. All elements have non-zero mass and inertia to avoid singularities in the equations of motion. A torque can be applied at the hip to generate leg reciprocation and telescopic actuation in the thigh allows leg-length control.

The parameter values used in this chapter are listed in Table E.1. The initial conditions to start the model in a periodic gait are provided in Table E.2.

E.2.2. Equations of Motion

The derivation of the equations of motion starts from the body, which has its centre of mass at the Cartesian coordinates $x_\mathrm{m}, z_\mathrm{m}$ and has a pitch angle θ_b.

Table E.1: Parameter choice for two-legged running model.

Parameter		Value	Unit
Body mass	m_b	$0.80^\star$	M
Body inertia	J_b	0.10^+	$\mathrm{M\,L^2}$
Thigh length	l_t	$0.70^\star$	L
Thigh mass	m_t	$0.08^\star$	M
Thigh inertia	J_t	$0.01^\star$	$\mathrm{M\,L^2}$
Shank length	l_s	$0.30^\star$	L
Shank mass	m_s	$0.01^\star$	M
Shank inertia	J_s	$0.005^\star$	$\mathrm{M\,L^2}$
Foot mass	m_f	$0.01^\star$	M
Hip offset	r_1	0.30^+	L
Leg CoM fraction	r_2	$0.40^\star$	–

$^+$ based on a fixed point from the TSLIP model
* result from the numerical search for a periodic gait
* fixed parameter

Table E.2: Initial conditions for the two-legged running model.

	Positions			Velocities		
Parameter		Value	Unit		Value	Unit
Horizontal body position	x_b	0.000^+	L	$\dot{x}_\mathrm{b}$	1.898^+	$\mathrm{g^{1/2}\,L^{1/2}}$
Vertical body position	z_b	0.514^+	L	$\dot{z}_\mathrm{b}$	-0.079^+	$\mathrm{g^{1/2}\,L^{1/2}}$
Body pitch angle	θ_b	-0.290^+	rad	$\dot{\theta}_\mathrm{b}$	0.202^*	$\mathrm{rad\,g^{1/2}\,L^{-1/2}}$
Right thigh length	$l_\mathrm{t,R}$	0.700^+	L	$\dot{l}_\mathrm{t,R}$	-0.012^*	$\mathrm{g^{1/2}\,L^{1/2}}$
Right shank length	$l_\mathrm{s,R}$	0.300^+	L	$\dot{l}_\mathrm{s,R}$	-0.886^*	$\mathrm{g^{1/2}\,L^{1/2}}$
Right hip angle	$\theta_\mathrm{h,R}$	-0.351^+	rad	$\dot{\theta}_\mathrm{h,R}$	1.6282^*	$\mathrm{rad\,g^{1/2}\,L^{-1/2}}$
Left thigh length	$l_\mathrm{t,L}$	0.370^*	L	$\dot{l}_\mathrm{t,L}$	-0.997^*	$\mathrm{g^{1/2}\,L^{1/2}}$
Left shank length	$l_\mathrm{s,L}$	$0.300^\star$	L	$\dot{l}_\mathrm{s,L}$	-0.136^*	$\mathrm{g^{1/2}\,L^{1/2}}$
Left hip angle	$\theta_\mathrm{h,L}$	0.690^*	rad	$\dot{\theta}_\mathrm{h,L}$	-2.9350^*	$\mathrm{rad\,g^{1/2}\,L^{-1/2}}$

$^+$ based on a fixed point from the TSLIP model
* result from the numerical search for a periodic gait
* fixed parameter

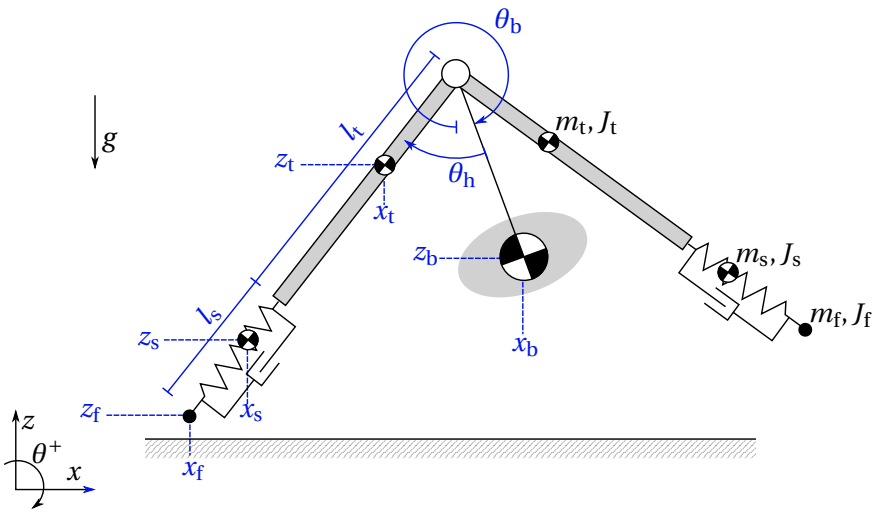

Figure E.1: Planar running model with two legs with non-zero mass. The body has a mass m_b and rotational moment of inertia J_b. A torque τ can be applied at each hip, to drive the rotation of the legs. The legs are identical and the subscripts "R" and "L" are used to distinguish forces and states between the two legs. The thigh with length l_t, mass m_t, and inertia J_t is telescopically actuated with a force F_t. The shank has length l_s, mass m_s, and inertia J_s. It is a linear spring-damper with force F_s. At the end of the shank is a point-mass foot with mass m_f. The ground reaction forces in vertical direction, F_z, and horizontal direction, F_x, are applied at the feet.

The rotation matrix $R(\theta)$ about an angle θ is

$$\mathbf{R}_y(\theta) = \begin{bmatrix} \cos(\theta) & \sin(\theta) \\ -\sin(\theta) & \cos(\theta) \end{bmatrix}, \tag{E.1}$$

which can be used to transform the unit vectors in the inertial reference frame $\boldsymbol{e}$ to the unit vectors in the body reference frame $\boldsymbol{b}$,

$$\boldsymbol{b}_z = \mathbf{R}_y(\theta_b)\boldsymbol{e}_z. \tag{E.2}$$

Next, define the hip reference frame $\boldsymbol{h}$ for each leg, rotated an angle θ_l from the body,

$$\boldsymbol{h}_{z,L} = \mathbf{R}_y(\theta_{h,L})\boldsymbol{b}_z, \qquad \boldsymbol{h}_{x,R} = \mathbf{R}_y(\theta_{h,R})\boldsymbol{b}_x. \tag{E.3}$$

The position vector $\boldsymbol{p}_b$ defines the centre-of-mass position of the body in the inertial reference frame,

$$\boldsymbol{p}_b = x_m\boldsymbol{e}_x + z_m\boldsymbol{e}_z. \tag{E.4}$$

The hip position $\boldsymbol{p}_h$ is then defined relative to the body,

$$\boldsymbol{p}_h = \boldsymbol{p}_b + r_1\boldsymbol{b}_z, \tag{E.5}$$

and the position of the centre of mass of the thigh, $\boldsymbol{p}_t$, the shank, $\boldsymbol{p}_s$, and the foot, $\boldsymbol{p}_f$, are defined relative to the hip point,

$$\boldsymbol{p}_{t,L} = \boldsymbol{p}_h - r_2 l_{t,L}\boldsymbol{h}_{z,L}, \qquad \boldsymbol{p}_{t,R} = \boldsymbol{p}_h - r_2 l_{t,R}\boldsymbol{h}_{z,R}, \tag{E.6}$$

$$\boldsymbol{p}_{s,L} = \boldsymbol{p}_h - (l_{t,L} + r_2 l_{s,L})\boldsymbol{h}_{z,L}, \qquad \boldsymbol{p}_{s,R} = \boldsymbol{p}_h - (l_{t,R} + r_2 l_{s,R})\boldsymbol{h}_{z,R}, \tag{E.7}$$

$$\boldsymbol{p}_{f,L} = \boldsymbol{p}_h - (l_{t,L} + l_{s,L})\boldsymbol{h}_{z,L}, \qquad \boldsymbol{p}_{t,R} = \boldsymbol{p}_h - (l_{t,R} + l_{s,R})\boldsymbol{h}_{z,R}, \tag{E.8}$$

where r_2 is the position of the centre of mass as a fraction of the length of the leg segment.

The minimal coordinate vector $\boldsymbol{q}$ fully describes the system configuration,

$$\boldsymbol{q} = \begin{bmatrix} x_\mathrm{b} & z_\mathrm{b} & \theta_\mathrm{b} & l_\mathrm{t,R} & l_\mathrm{s,R} & \theta_\mathrm{h,R} & l_\mathrm{t,L} & l_\mathrm{s,L} & \theta_\mathrm{h,L} \end{bmatrix}^\mathrm{T}. \tag{E.9}$$

The kinematic transformation full system coordinate vector $\boldsymbol{T}(\boldsymbol{q}) : \mathbb{R}^9 \rightarrow \mathbb{R}^{27}$ describes the transformation form minimal coordinates to the full set of coordinates,

$$\begin{aligned} \boldsymbol{x} = \boldsymbol{T}(\boldsymbol{q}) = \Big[& \boldsymbol{p}_\mathrm{b}^\mathrm{T} \quad \theta_\mathrm{b} \quad \boldsymbol{p}_\mathrm{h}^\mathrm{T} \\ & \boldsymbol{p}_\mathrm{t,R}^\mathrm{T} \quad \theta_\mathrm{t,R} \quad \boldsymbol{p}_\mathrm{s,R}^\mathrm{T} \quad \theta_\mathrm{s,R} \quad l_\mathrm{R} \quad l_\mathrm{t,R} \quad l_\mathrm{s,R} \\ & \boldsymbol{p}_\mathrm{t,L}^\mathrm{T} \quad \theta_\mathrm{t,L} \quad \boldsymbol{p}_\mathrm{s,L}^\mathrm{T} \quad \theta_\mathrm{s,L} \quad l_\mathrm{L} \quad l_\mathrm{t,L} \quad l_\mathrm{s,L} \\ & \boldsymbol{p}_\mathrm{f,R}^\mathrm{T} \quad \boldsymbol{p}_\mathrm{f,L}^\mathrm{T} \Big]^\mathrm{T}. \end{aligned} \tag{E.10}$$

The Jacobian of the kinematic transformation $\mathbf{J}_\mathrm{T}$ is taken with respect to the minimal coordinates,

$$\mathbf{J}_\mathrm{T}(\boldsymbol{q}) = \frac{\partial \mathbf{T}(\boldsymbol{q})}{\partial \boldsymbol{q}}. \tag{E.11}$$

This Jacobian allows the computation of the full set of velocities $\dot{\boldsymbol{x}}$ from the minimal velocities $\dot{\boldsymbol{q}}$,

$$\dot{\boldsymbol{x}} = \mathbf{J}_\mathrm{T}(\boldsymbol{q})\,\dot{\boldsymbol{q}}. \tag{E.12}$$

The full mass matrix $\mathbf{M}_\mathrm{f}$ is a diagonal matrix with the body mass m and mass moment of inertia J,

$$\begin{aligned} \mathbf{M}_\mathrm{f} = \mathrm{diag}\Big[& m_\mathrm{b} \quad m_\mathrm{b} \quad J_\mathrm{b} \quad 0 \quad 0 \\ & m_\mathrm{t} \quad m_\mathrm{t} \quad J_\mathrm{t} \quad m_\mathrm{s} \quad m_\mathrm{s} \quad J_\mathrm{t} \quad 0 \quad 0 \quad 0 \\ & m_\mathrm{t} \quad m_\mathrm{t} \quad J_\mathrm{t} \quad m_\mathrm{s} \quad m_\mathrm{s} \quad J_\mathrm{t} \quad 0 \quad 0 \quad 0 \\ & m_\mathrm{f} \quad m_\mathrm{f} \quad m_\mathrm{f} \quad m_\mathrm{f} \Big] \end{aligned} \tag{E.13}$$

This is reduced to the mass matrix in minimal coordinates $\mathbf{M}$ with the kinematic Jacobian,

$$\mathbf{M} = \mathbf{J}_\mathrm{T}^\mathrm{T} \mathbf{M}_\mathrm{f} \mathbf{J}_\mathrm{T}. \tag{E.14}$$

The force vectors are defined in the full set of coordinates. The gravitational acceleration g acts downward along the z axis. The applied force vector due to gravity $\boldsymbol{f}_\mathrm{g}$ is then

$$\begin{aligned} \boldsymbol{f}_\mathrm{g} = \Big[& 0 \quad -m_\mathrm{b} g \quad 0 \quad 0 \quad 0 \\ & 0 \quad -m_\mathrm{t} g \quad 0 \quad 0 \quad -m_\mathrm{s} g \quad 0 \quad 0 \quad 0 \quad 0 \\ & 0 \quad -m_\mathrm{t} g \quad 0 \quad 0 \quad -m_\mathrm{s} g \quad 0 \quad 0 \quad 0 \quad 0 \\ & 0 \quad -m_\mathrm{f} g \quad 0 \quad -m_\mathrm{f} g \Big]. \end{aligned} \tag{E.15}$$

The vector $\boldsymbol{f}_\mathrm{grf}$ contains the forces applied at the feet when in contact with the ground,

$$\begin{aligned} \boldsymbol{f}_\mathrm{grf} = \Big[& 0 \quad 0 \quad 0 \quad 0 \quad 0 \\ & 0 \quad 0 \quad 0 \quad 0 \quad 0 \quad 0 \quad 0 \quad 0 \quad 0 \\ & 0 \quad 0 \quad 0 \quad 0 \quad 0 \quad 0 \quad 0 \quad 0 \quad 0 \\ & F_\mathrm{x,R} \quad F_\mathrm{z,R} \quad F_\mathrm{x,L} \quad F_\mathrm{z,L} \Big]. \end{aligned} \tag{E.16}$$

The vector $\boldsymbol{f}_\mathrm{a}$ contains the torque τ at the hip, the thigh force F_t and the shank force F_s,

$$\begin{aligned}\boldsymbol{f}_\mathrm{a} = \Big[& 0 \quad 0 \quad 0 \quad 0 \quad 0 \\ & 0 \quad 0 \quad \tau_\mathrm{R} \quad 0 \quad 0 \quad 0 \quad 0 \quad F_\mathrm{t,R} \quad F_\mathrm{s,R} \\ & 0 \quad 0 \quad \tau_\mathrm{L} \quad 0 \quad 0 \quad 0 \quad 0 \quad F_\mathrm{t,L} \quad F_\mathrm{s,L} \\ & 0 \quad 0 \quad 0 \quad 0 \Big] \,. \end{aligned} \tag{E.17}$$

The sum of the force vectors is transformed to the force vector in minimal coordinates $\boldsymbol{Q}$ with the kinematic Jacobian,

$$\boldsymbol{Q} = \mathbf{J}_\mathrm{T}^\mathrm{T}(\boldsymbol{f}_\mathrm{g} + \boldsymbol{f}_\mathrm{grf} + \boldsymbol{f}_\mathrm{a}) \,. \tag{E.18}$$

The sum of the force vectors is transformed to the force vector in minimal coordinates $\boldsymbol{Q}$ with the kinematic Jacobian,

$$\boldsymbol{Q} = \mathbf{J}_\mathrm{T}^\mathrm{T}(\boldsymbol{f}_\mathrm{g} + \boldsymbol{f}_\mathrm{t} + \boldsymbol{f}_\mathrm{l}) \,. \tag{E.19}$$

The convective accelerations $\boldsymbol{c}$ are computed,

$$\boldsymbol{c} = \left(\left(\frac{\partial \mathbf{J}_\mathrm{T}}{\partial \boldsymbol{q}} \right) \dot{\boldsymbol{q}} \right) \dot{\boldsymbol{q}} \,, \tag{E.20}$$

and transformed to the convective accelerations in minimal coordinates $\boldsymbol{C}$,

$$\boldsymbol{C} = \mathbf{J}_\mathrm{T}^\mathrm{T} \mathbf{M} \boldsymbol{c} \,. \tag{E.21}$$

The system of equations can be solved for the generalized accelerations $\ddot{\boldsymbol{q}}$ in stance,

$$\mathbf{M} \ddot{\boldsymbol{q}} = \boldsymbol{Q} - \boldsymbol{C} \,. \tag{E.22}$$

E.2.3. Ground Contact

A stiff, linear spring-damper model is used for to model the ground reaction forces. This model has a vertical stiffness k_z and damping c_z, and a horizontal stiffness k_x and damping c_x. The displacement is specified with respect to the touch-down position of the foot, which is denoted with the subscript "TD". The foot is not allowed to pull on the ground, so the ground reaction forces are only applied if the vertical force is larger than zero,

$$F_\mathrm{z} = \begin{cases} k_\mathrm{z}(z_\mathrm{f,TD} - z_\mathrm{f}) - c_\mathrm{z} \dot{z}_\mathrm{f} & \text{if } F_\mathrm{z} > 0 \wedge z_\mathrm{f} \leq 0 \,, \\ 0 & \text{otherwise,} \end{cases} \tag{E.23}$$

$$F_\mathrm{x} = \begin{cases} k_\mathrm{x}(x_\mathrm{f,TD} - x_\mathrm{f}) - c_\mathrm{x} \dot{x}_\mathrm{f} & \text{if } F_\mathrm{z} > 0 \wedge z_\mathrm{f} \leq 0 \,, \\ 0 & \text{otherwise.} \end{cases} \tag{E.24}$$

E.2.4. Actuation and Control

Motivated by the robustness of the TSLIP model response, we design simple parametric trajectories to generate the required leg reciprocation. The parameters for the controller are listed in Table E.4.

Table E.3: Ground contact model parameters.

Parameter		Value	Unit
Vertical ground stiffness	k_z	100.0	$M\,g\,L^{-1}$
Vertical ground damping	c_z	10.0	$M\,g^{1/2}\,L^{-1/2}$
Horizontal ground stiffness	k_x	200.0	$M\,g\,L^{-1}$
Horizontal ground damping	c_x	20.0	$M\,g^{1/2}\,L^{-1/2}$

Table E.4: Controller parameters for the two-legged running model.

Parameter		Value	Unit
Duty factor	d	0.58^{+}	–
Stride time	T	1.40^{+}	$g^{-1/2}\,L^{1/2}$
Initial phase offset	ρ_0	0.08^{*}	–
Thigh proportional gain	$K_{p,t}$	$500.0^{\star}$	$M\,g\,L^{-1}$
Thigh derivative gain	$K_{d,t}$	$20.0^{\star}$	$M\,g^{1/2}\,L^{-1/2}$
Thigh length in swing	$l_{t,s}$	$0.40^{\star}$	L
Hip proportional gain	$K_{p,\theta}$	$0.50^{\star}$	$M\,g\,L\,rad^{-1}$
Hip derivative gain	$K_{d,\theta}$	$0.50^{\star}$	$M\,g^{1/2}\,L^{3/2}\,rad^{-1}$
Hip angle forward reference	θ_f	-0.54^{*}	rad
Hip angle sweep	θ_s	1.44^{*}	rad
Shank spring stiffness	k	8.0^{+}	$M\,g\,L^{-1}$
Shank spring damping	c_l	0.30^{+}	$M\,g^{1/2}\,L^{-1/2}$

$^{+}$ based on a fixed point from the TSLIP model

* result from the numerical search for a periodic gait

* fixed parameter

Phase definition

Define a phase variable $\rho \in [0,1)$, which determines the phase in the stride period T.

$$\rho = \frac{t \bmod T}{T}. \tag{E.25}$$

The phase of the right leg ρ_{R} is shifted by an initial offset ρ_0. The phase of the left leg $\rho_{\mathrm{L}}$is shifted a half period from the right leg,

$$\rho_{\mathrm{R}} = (\rho + \rho_0) \bmod 1, \tag{E.26}$$

$$\rho_{\mathrm{L}} = (\rho_{\mathrm{R}} + 0.5) \bmod 1. \tag{E.27}$$

Compliant Shank Behaviour

The shank provides the compliant function required for the stance-phase behaviour. It functions as a linear spring-damper with stiffness k, resting length $l_{\mathrm{s},0}$, and damping coefficient c_{l},

$$F_{\mathrm{s}} = k(l_{\mathrm{s},0} - l_{\mathrm{s}}) - c_{\mathrm{l}}\dot{l}_{\mathrm{s}} \tag{E.28}$$

Thigh-Length Control

The thigh-length reference $l_{\mathrm{t,ref}}$ is set to a constant value of $l_{\mathrm{t},0}$ during the stance phase to not interfere with the effect of the shank compliance. During the swing phase, the thigh needs to be shortened to provide ground clearance. The leg is retracted to a length $l_{\mathrm{t,s}}$, with a parabolic reference trajectory that starts and ends at the stance-phase reference length,

$$l_{\mathrm{t,ref}}(\rho) = \begin{cases} l_{\mathrm{t},0} & \text{if } \rho \le d, \\ l_{\mathrm{t,s}}\left(\frac{2\rho-1-d}{1-d}\right)^2 + \left(l_{\mathrm{t},0} - l_{\mathrm{t,s}}\right) & \text{otherwise.} \end{cases} \tag{E.29}$$

The reference leg-length velocity of the thigh is set to the time derivative of the position reference,

$$\dot{l}_{\mathrm{t,ref}} \begin{cases} 0 & \text{if } \rho \le d, \\ \frac{4l_{\mathrm{t,s}}}{1-d}\left(\frac{2\rho-1-d}{1-d}\right)\frac{1}{T} & \text{otherwise.} \end{cases} \tag{E.30}$$

The force F_{t} applied by the thigh controller is then calculated with the reference trajectories,

$$F_{\mathrm{t}}(\rho) = K_{\mathrm{p,t}}(l_{\mathrm{t,ref}}(\rho) - l_{\mathrm{t,ref}}) + K_{\mathrm{d,t}}(\dot{l}_{\mathrm{t,ref}}(\rho) - \dot{l}_{\mathrm{t,ref}}), \tag{E.31}$$

where $K_{\mathrm{p,t}} \ge 0$ is the proportional gain and $K_{\mathrm{d,t}} \ge 0$ is the derivative gain.

Hip-Angle Control

The reciprocating behaviour of the legs is generated from the reference trajectory for the hip angle θ_{ref}.

$$\theta_{\mathrm{ref}}(\rho) = \begin{cases} -\frac{\theta_{\mathrm{s}}}{2}\left[\cos\left(\frac{\rho\pi}{d}\right) + 1\right] + \theta_{\mathrm{f}} & \text{if } \rho \le d, \\ \frac{\theta_{\mathrm{s}}}{2}\left[\cos\left(\frac{(\rho-d)\pi}{(1-d)}\right) + 1\right] + \theta_{\mathrm{f}} & \text{otherwise.} \end{cases} \tag{E.32}$$

This prescribes leg retraction from the forward angle θ_f through a sweep angle θ_s for the stance phase. The swing-phase trajectory brings the leg forward again for the next step. The velocity reference for the hip angle controller $\dot{\theta}_\mathrm{ref}$ is the time derivative of the position reference,

$$\dot{\theta}_\mathrm{ref}(\rho) = \begin{cases} \frac{\pi}{d} \cdot \frac{\theta_\mathrm{s}}{2} \sin\left(\frac{\rho\pi}{d}\right) \frac{1}{T} & \text{if } \rho \leq d\,, \\ -\frac{\pi}{(1-d)} \cdot \frac{\theta_\mathrm{s}}{2} \sin\left(\frac{(\rho-d)\pi}{(1-d)}\right) \frac{1}{T} & \text{otherwise.} \end{cases} \tag{E.33}$$

The hip torque is then calculated with the reference trajectories,

$$\tau(\rho) = K_{\mathrm{p},\theta}(\theta_\mathrm{ref}(\rho) - \theta) + K_{\mathrm{d},\theta}(\dot{\theta}_\mathrm{ref}(\rho) - \dot{\theta})\,, \tag{E.34}$$

where $K_{\mathrm{p},\theta} \geq 0$ is the proportional gain and $K_{\mathrm{d},\theta} \geq 0$ is the derivative gain.

E.2.5. Numerical Integration

The equations of motion are numerically integrated with a Dormand-Prince 5(4) embedded Runge-Kutta integrator (Dormand and Prince, 1980) in Java, as implemented in Apache Commons Math 3.6. Absolute and relative tolerance on the integrated state are set to 1.0×10^{-8} in dimensionless units as per Table 3.1. The touch-down of the right foot is implemented as a switching condition to mark the beginning and end of the stride.

E.2.6. Search for Periodic Gaits

The search for periodic limit cycles of the two-legged running model covers both control parameters and initial conditions. The initial guess makes use of a fixed point for the TSLIP model. Parameters that can be directly implemented in the two-legged model are fixed in the optimization to minimize the number of free variables.

The model variables are thus either chosen, based on the TSLIP result, or free in the optimization. This distinction is indicated in the tables with the model configuration in Table E.1, controller parameters in Table E.2.4, and initial conditions in Table E.2.

Periodic limit cycles are found by numerical optimization, with a method similar to that applied in the TSLIP study. A Covariant Matrix Adaptation Evolution Strategy (CMAES) (Hansen et al., 2009) optimization is applied to minimize the cost function, implemented with the Apache Commons Math 3.6 library in Java.

We combine the system configuration in minimal coordinates, $\boldsymbol{q}$, and velocities, $\dot{\boldsymbol{q}}$, into a state vector $\boldsymbol{z}$. The horizontal position x_b is not periodic and therefore the first element is removed from the state vector. The cost function $C(\boldsymbol{z})$ for finding a fixed point takes the sum of squared differences over one stride,

$$\boldsymbol{z} = \begin{bmatrix} \boldsymbol{x} \\ \dot{\boldsymbol{x}} \end{bmatrix}, \tag{E.35}$$

$$C(\boldsymbol{z}) = (\boldsymbol{z}_n - \boldsymbol{z}_{n+1})^\mathrm{T}(\boldsymbol{z}_n - \boldsymbol{z}_{n+1})\,. \tag{E.36}$$

The initial state $\boldsymbol{z}_n$ is set to always start at the beginning of the stance phase with the right foot on the ground. The state after one stride $\boldsymbol{z}_{n+1}$ is the result of numerically integrating a full stride and taking the system state immediately after touch-down of the right foot.

E.3. Methods

E.3.1. Reciprocating Leg Controller

The controller performance is tested by comparing the actual joint trajectories to the reference trajectories. The thigh length is expected to follow closely due to the high-gain controller, whereas the hip angle is expected to deviate more from the trajectory due to the lower gains on the controller. The shank is expected to show similar behaviour to the leg spring in the TSLIP model.

E.3.2. Stability and Robustness

The model is expected to inherit some of the properties in stability and robustness from the TSLIP model that is used as a basis. We test for stability with the eigenvalues of the linearized stride-to-stride map, defining a stride from the touch-down of the right foot to the next touch-down of the right foot. Robustness is evaluated as the number of full strides the model runs until falling.

E.3.3. Metacentric Pitch Stabilization

We test for metacentric stabilization of body pitch in a manner similar to the test for the TSLIP model. The ground reaction forces and resultant impulse are compared for a change in body-pitch angle, θ_{b}, of 0.0 rad, 0.5 rad, and –0.5 rad. The leg position and orientation are not changed with respect to the inertial reference frame. To that effect, the hip angles, θ_{h}, are adjusted in the opposite direction of the leg angle.

E.4. Results

E.4.1. Reciprocating Leg Controller

The search for a periodic gait results in a viable running gait for the two-legged model, using the TSLIP model for a starting point and parametric trajectories for control.

The reference trajectories for generating the reciprocating bipedal running behaviour are plotted in Figure E.2 together with the actual trajectories in simulation. The thigh length and velocity closely follow the trajectory as controlled by the high-gain PD controller. The shank exhibits simple spring-damper behaviour. It shortens and then extends as the runner moves through the stance phase, followed by a damped oscillation in the swing phase. The hip angle deviates more from the reference trajectory than the thigh length. There are some sharp changes in hip angular velocity upon touch-down and lift-off.

Figure E.3 shows how the joint-space trajectories correspond to a reference foot trajectory and the actual foot trajectory. The foot trajectories are not perfectly periodic.

E.4.2. Stability and Robustness

The gait is numerically unstable from these initial conditions, with a maximum eigenvalue of 67.0. The model falls after approximately 10 full strides. The last strides before the model falls, the hip angles for both legs start to deviate more from the reference trajectory.

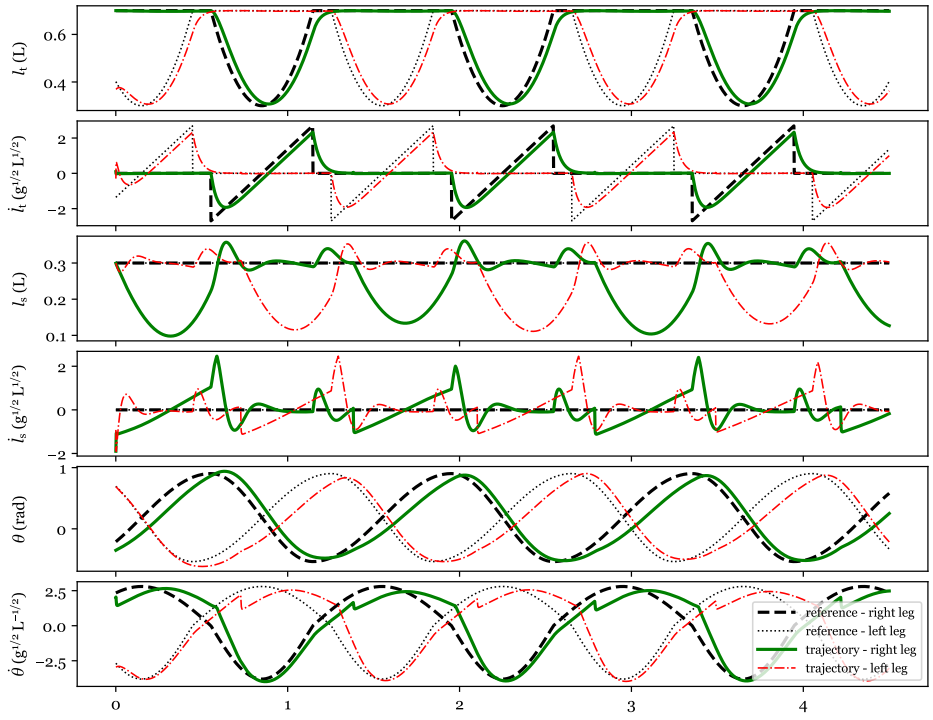

Figure E.2: Controller reference and recorded trajectories for thigh length l_t, shank length l_s and hip angle θ_h of the two-legged planar running model.

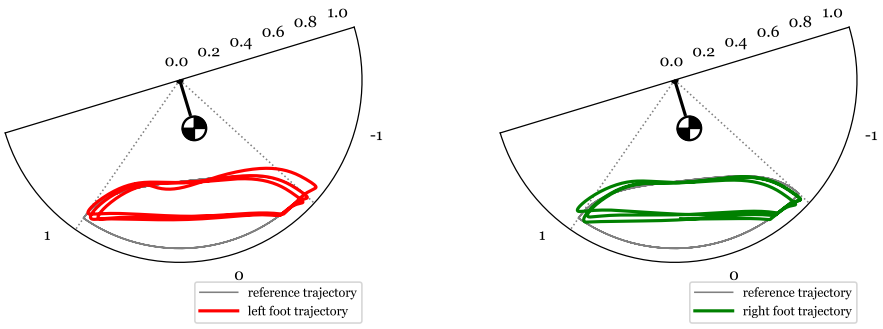

Figure E.3: Reference trajectory and actual trajectory of the foot. The coordinate system is centred at the hip. The actual trajectory deviates from the reference during stance due to the compliance of the lower leg.

E.4.3. Metacentric Pitch Stabilization

The ground reaction forces remain mostly unchanged in response to a disturbance in body pitch as illustrated in Figure E.4. The resultant impulse from the ground reaction forces provides a restoring torque about the centre of mass. The magnitude and direction of the impulse show only little change from the change in body-pitch angle.

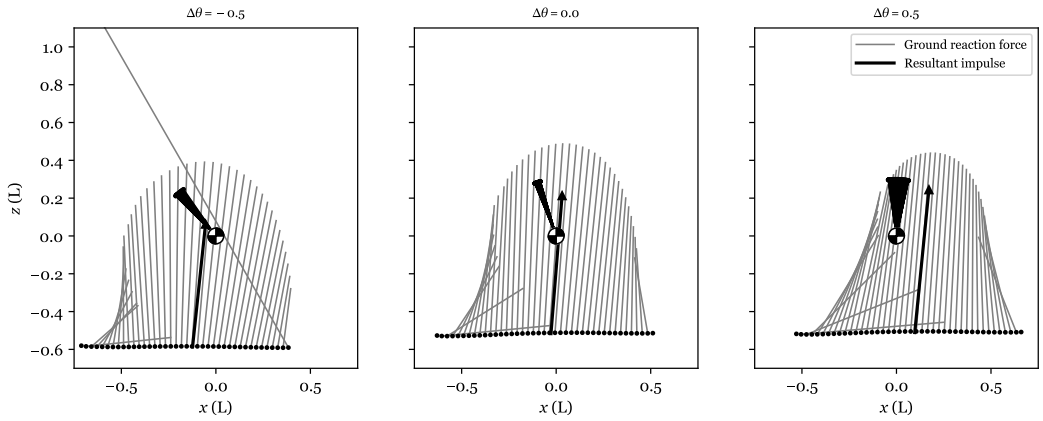

Figure E.4: Change in ground reaction force and resultant impulse for a disturbance in body pitch.

E.5. Discussion

The results with the two-legged model confirm that it is feasible to use a simple template model as an anchor for a more complex running model. Parallels in model design provide a good starting point for search for a periodic gait, starting from a configuration that is expected to be viable limits the number of free parameters.

The control for this model is designed to provide a means of leg reciprocation for bipedal running. These simple parametric trajectories enable bipedal running for the model with leg mass. It supports the ideas that underly the Planar Elliptical Runner, that fast bipedal running does not require complex control - robust planar running can follow from the system dynamics.

Although the resulting gait is not perfectly periodic and numerically unstable, we do observe that the metacentric model is applicable to the body-pitch stabilization of the two-legged model. This conservation of pitch-stabilization and the basic viability of the running gait shows that properties of the simple model can be retained as model complexity increases, even though stability and robustness may not be fully conserved.

Optimization methods using more information from the dynamics may yield better solutions in terms of accuracy of the periodic gait and stability, with less computational power than the single-shooting evolution strategy that was applied.

A future step may be the development of a planar running robot that is designed based on simulation parameters. This could validate the design of experimental robot dynamics building on simplified model results.

E.6. Conclusion

Simple models for bipedal running may be used to model the centre-of-mass dynamics and other gait dynamics. Conversely, simple models can be used as a foundation for robotic design. We show that the TSLIP model provides a good starting point for design of a two-legged running model with a trunk and non-massless legs. Simple parametric trajectories can be used to generate a bipedal running gait in this model. Metacentric self-stabilization of body pitch is conserved, as is the basic viability of the running gait, however the gait does become unstable and less robust than that of the TSLIP model it is built upon.

F

Credits

This chapter provides credit where credit is due for the ideas in this thesis, such that it may be clear which is my own work and where I borrow from the unpublished work of colleagues.

Johnny Godowski provided the intuitive ideas that underly the metacentric stability described in the paper, describing pitch stabilization as metacentric buoyancy related a hanging body-mass configuration and an elliptical foot trajectory. He provided the idea that a forward body-pitch angle was related to accelerated running. The HexRunner was developed and experimented wiuth by Sebastian Cotton, Colton Black, Nick Payton, Ionut Olaru, Johnny Godowski and Chris Schmidt-Wetekam. They later used intuitive understanding of the dynamics and mechanical design to construct the Planar Elliptical Runner. The robot is testament to the possible robustness of fast planar bipedal running, as it was designed with only minimal background in simulation.

Jerry Pratt has been the driving force in trying to provide more understandable and testable explanations. He has been the key to converting the intuition that underlies the Planar Elliptical Runner into more tangible questions and approachable problems.

Under his supervision, Ken Chao performed a preliminary study to replicate the self-stable behaviours found in the SLIP model. He found some evidence for the decoupling of foot placement and centre-of-mass motion at high velocities. He constructed a precursor to the TSLIP model by adding a pendulum to the hip of the standard SLIP model to begin capturing the problem of trunk stabilization. This model exhibited self-stable gaits but still relied on inertial measurements.

I started the work for my thesis with this SLIP model with a pendulum extension, but found it had a singular configuration for the pendulum length $r = 0.0$. Therefore, I made the transition to the TSLIP model based on use in literature (van Oijen et al., 2013) as it did not have this singularity. The derivation of the equations of motion and the code for numerical integration, limit-cycle search, testing stability and robustness were fully done by me, as are all the graphs and illustrations in this thesis.

I formulated the hypotheses in the paper after discussing with Jerry Pratt the concepts that needed to be tested and explained. Furthermore, I set up the methods for testing the hypotheses. Jerry suggested looking at the resultant ground impulse per step to test for metacentric stability. I implemented the methods and further made the comparison to the virtual pendulum models (Maus et al., 2010). Jerry suggested that I look into the stance-phase interaction

between the leg spring and the centre-of-mass trajectory to find out more about height and velocity stabilization; he proposed they could be stable without damping based on discussions with Johnny Godowski and Chris Schmidt-Wetekam. I made the choice to evaluate the contributions of both leg and hip damping, as well as which parameters sweeps I performed. I made the choice for the control strategies in the model with feedback from Jerry.

It was my own idea to use motion tracking for performing measurements on the Planar Elliptical Runner. Chris Schmidt-Wetekam operated the robot during the experiment and Billy Howell set up the camera and lighting. I then used the high-speed video to perform the motion tracking on the feet and body markers of the robot. I then also processed and filtered this data and graphed the per-step averages. I fitted the TSLIP model to these measurements and quantified the quality of the model fit.

Finally I wrote up the paper to combine all ideas, results, and discussion into a single document to be published. Jerry Pratt, Heike Vallery, Chris Schmidt-Wetekam, Johnny Godowski and Robert Griffin provided feedback on the writing.

The work in the appendices is mostly mine, I designed a two-legged running model to build on the TSLIP model for planar running. I do have to thank Sylvain Bertrand for suggesting to start with a planar two-legged model, instead of making the jump to three-dimensional running directly from the TSLIP. I derived the equations of motion, designed the parametric controller, and wrote the code for integration and optimization.

Bibliography

Ahmadi, M. and Buehler, M. (2006). Controlled passive dynamic running experiments with the ARL-Monopod II. *IEEE Trans. Robot.*, 22(5):974–986.

Andrada, E., Rode, C., and Blickhan, R. (2013). Grounded running in quails: Simulations indicate benefits of observed fixed aperture angle between legs before touch-down. *J. Theor. Biol.*, 335:97–107.

Bertrand, S. (2012). *A Control Strategy for High-Speed Running within Unknown Environments for a 3D Bipedal Robot*. PhD thesis, UVSQ.

Birn-Jeffery, A. V., Hubicki, C. M., Blum, Y., Renjewski, D., Hurst, J. W., and Daley, M. A. (2014). Don't break a leg: running birds from quail to ostrich prioritise leg safety and economy on uneven terrain. *J. Exp. Biol.*, 217(21):3786–3796.

Blickhan, R. (1989). The spring-mass model for running and hopping. *J. Biomech.*, 22(11-12):1217–1227.

Blum, Y., Birn-Jeffery, A., Daley, M. A., and Seyfarth, A. (2011). Does a crouched leg posture enhance running stability and robustness? *J. Theor. Biol.*, 281(1):97–106.

Blum, Y., Vejdani, H. R., Birn-Jeffery, A. V., Hubicki, C. M., Hurst, J. W., and Daley, M. A. (2014). Swing-Leg Trajectory of Running Guinea Fowl Suggests Task-Level Priority of Force Regulation Rather than Disturbance Rejection. *PLoS One*, 9(6).

Cotton, S., Mihai, I., Olaru, C., Bellman, M., van der Ven, T., Godowski, J., and Pratt, J. (2012). FastRunner: A Fast, Efficient and Robust Bipedal Robot. Concept and Planar Simulation. In *2012 IEEE Int. Conf. Robot. Autom.*, pages 2358–2364. IEEE.

Daley, M. A. and Usherwood, J. R. (2010). Two explanations for the compliant running paradox: reduced work of bouncing viscera and increased stability in uneven terrain. *Biol. Lett.*, 6(3):418–421.

Dormand, J. R. and Prince, P. J. (1980). A family of embedded Runge-Kutta formulae. *J. Comput. Appl. Math.*, 6(1):19–26.

Ernst, M., Geyer, H., and Blickhan, R. (2012). Extension and customization of self-stability control in compliant legged systems. *Bioinspiration and Biomimetics*, 7(4):046002.

Geyer, H., Seyfarth, A., and Blickhan, R. (2006). Compliant leg behaviour explains basic dynamics of walking and running. *Proc. R. Soc. B Biol. Sci.*, 273(1603):2861–2867.

Ghigliazza, R. M., Altendorfer, R., Holmes, P., and Koditschek, D. (2003). A Simply Stabilized Running Model. *SIAM J. Appl. Dyn. Syst.*, 2(2):187–218.

Grizzle, J. W., Hurst, J., Morris, B., Park, H. W., and Sreenath, K. (2009). MABEL, a new robotic bipedal walker and runner. In *Proc. Am. Control Conf.*, pages 2030–2036. IEEE.

Hackert, R., Schilling, N., and Fischer, M. S. (2006). Mechanical self-stabilization, a working hypothesis for the study of the evolution of body proportions in terrestrial mammals? *C. R. Palevol*, 5(3-4):541–549.

Hansen, N., Niederberger, A. S. P., Guzzella, L., and Koumoutsakos, P. (2009). A Method for Handling Uncertainty in Evolutionary Optimization With an Application to Feedback Control of Combustion. 13(1):180–197.

Hosoda, K., Takuma, T., Nakamoto, A., and Hayashi, S. (2008). Biped robot design powered by antagonistic pneumatic actuators for multi-modal locomotion. *Rob. Auton. Syst.*, 56(1):46–53.

Hubicki, C., Grimes, J., Jones, M., Renjewski, D., Sproewitz, A., Abate, A., and Hurst, J. (2016). ATRIAS: Design and validation of a tether-free 3D-capable spring-mass bipedal robot. *Int. J. Rob. Res.*, 35(12):1497–1521.

Karssen, D. and Wisse, M. (2011). Running with improved disturbance rejection by using non-linear leg springs. *Int. J. Rob. Res.*, 30(13):1585–1595.

Karssen, J. G. D., Haberland, M., Wisse, M., and Kim, S. (2015). The effects of swing-leg retraction on running performance: analysis, simulation, and experiment. *Robotica*, 33(10):2137–2155.

Kim, S., Kim, K.-S., Kim, Y. K., Yoon, B., and Park, J. (2014). Design of biped robot inspired by cats for fast running. *Electron. Lett.*, 50(10):730–731.

Maus, H. M., Lipfert, S. W., Gross, M., Rummel, J., and Seyfarth, A. (2010). Upright human gait did not provide a major mechanical challenge for our ancestors. *Nat. Commun.*, 1.

Maus, H.-M., Rummel, J., and Seyfarth, A. (2008). Stable upright walking and running using a simple pendulum based control scheme. In *Proc. 11th Int. Conf. Climbing Walk. Robot. Support Technol. Mob. Mach.*, pages 623–629.

McGeer, T. (1990). Passive bipedal running. *Proc. R. Soc. B Biol. Sci.*, 240(1297):107–134.

McMahon, T. A. and Bonner, J. T. (1983). *On Size and Life*. Scientific American, New York.

McMahon, T. A. and Cheng, G. C. (1990). The mechanics of running: How does stiffness couple with speed? *J. Biomech.*, 23(SUPPL. 1):65–78.

Mombaur, K. D. (2009). Using optimization to create self-stable human-like running. *Robotica*, 27(3):321–330.

Mombaur, K. D., Longman, R. W., Bock, H. G., and Schlöder, J. P. (2005). Open-loop stable running. *Robotica*, 23(1):21–33.

Morris, B., Westervelt, E. R., Chevallereau, C., Buche, G., and Grizzle, J. W. (2006). Achieving bipedal running with RABBIT: Six steps toward infinity. In *Fast Motions Biomech. Robot. Optim. Control*, volume 340, pages 277–297.

Neville, N., Buehler, M., and Sharf, I. (2006). A bipedal running robot with one actuator per leg. *Proc. - IEEE Int. Conf. Robot. Autom.*, 2006(May):848–853.

Owaki, D., Koyama, M., Yamaguchi, S., Kubo, S., and Ishiguro, A. (2011). A 2-D Passive-Dynamic-Running Biped With Elastic Elements. *IEEE Trans. Robot.*, 27(1):156–162.

Palmer, L. R., Eaton, C. E., Palmer III, L. R., and Eaton, C. E. (2014). Periodic spring-mass running over uneven terrain through feedforward control of landing conditions. *Bioinspiration and Biomimetics*, 9(3):036018.

Parker, T. S. and Chua, L. O. (1989). *Practical Numerical Algorithms for Chaotic Systems*. Springer Verlag, New York.

Peuker, F., Seyfarth, A., and Grimmer, S. (2012). Inheritance of SLIP running stability to a single-legged and bipedal model with leg mass and damping. In *2012 4TH IEEE RAS EMBS Int. Conf. Biomed. Robot. Biomechatronics*, pages 395–400. IEEE; RAS; EMBS.

Poulakakis, I. and Grizzle, J. W. (2009). The spring loaded inverted pendulum as the hybrid zero dynamics of an asymmetric hopper. *IEEE Trans. Automat. Contr.*, 54(8):1779–1793.

Raibert, M. (1986). Legged Robots. *Commun. ACM*, 29(6):499–514.

Rashty, A. M. N., Sharbafi, M. A., Seyfarth, A., Mohammadi Nejad Rashty, A., Sharbafi, M. A., and Seyfarth, A. (2014). SLIP with swing leg augmentation as a model for running. In *IEEE Int. Conf. Intell. Robot. Syst.*, pages 2543–2549. IEEE.

Ringrose, R. (1997). Self-stabilizing running. In *Proc. Int. Conf. Robot. Autom.*, volume 1, pages 487–493. IEEE.

Savitzky, A. and Golay, M. J. (1964). Smoothing and Differentiation of Data by Simplified Least Squares Procedures. *Anal. Chem.*, 36(8):1627–1639.

Seyfarth, A. (2003). Swing-leg retraction: a simple control model for stable running. *J. Exp. Biol.*, 206(15):2547–2555.

Seyfarth, A., Geyer, H., Günther, M., and Blickhan, R. (2002). A movement criterion for running. *J. Biomech.*

Sharbafi, M. A., Ahmadabadi, M. N., Yazdanpanah, M. J., Nejad, A. M., and Seyfarth, A. (2013). Compliant hip function simplifies control for hopping and running. In *2013 IEEE/RSJ Int. Conf. Intell. Robot. Syst.*, pages 5127–5133. IEEE.

Shen, Z. H., Larson, P. L., and Seipel, J. E. (2014). Rotary and radial forcing effects on center-of-mass locomotion dynamics. *Bioinspiration and Biomimetics*, 9(3).

Taga, G., Yamaguchi, Y., and Shimizu, H. (1991). Self-organized control of bipedal locomotion by neural oscillators in unpredictable environment. *Biol. Cybern.*, 65(3):147–159.

Vallery, H. and Schwab, A. L. (2019). *Advanced Dynamics*. 2nd edition.

van Oijen, T. P., Karssen, J. G. D., and Wisse, M. (2013). The Effect of Center of Mass Offset on the Disturbance Rejection of Running Robots. *Int. J. Humanoid Robot.*, 10(02):1350004.